Aalborg Universitet

AALBORG UNIVERSITY
DENMARK

Amorphous Materials for Lithium-Ion and Post-Lithium-Ion Batteries

Ding, Junwei; Ji, Dongfang; Yue, Yuanzheng; Smedskjaer, Morten M.

Published in:
Small

DOI (link to publication from Publisher):
10.1002/smll.202304270

Creative Commons License
CC BY 4.0

Publication date:
2024

Document Version
Publisher's PDF, also known as Version of record

Link to publication from Aalborg University

Citation for published version (APA):
Ding, J., Ji, D., Yue, Y., & Smedskjaer, M. M. (2024). Amorphous Materials for Lithium-Ion and Post-Lithium-Ion Batteries. *Small*, *20*(5), Article 2304270. https://doi.org/10.1002/smll.202304270

General rights
Copyright and moral rights for the publications made accessible in the public portal are retained by the authors and/or other copyright owners and it is a condition of accessing publications that users recognise and abide by the legal requirements associated with these rights.

- Users may download and print one copy of any publication from the public portal for the purpose of private study or research.
- You may not further distribute the material or use it for any profit-making activity or commercial gain
- You may freely distribute the URL identifying the publication in the public portal -

Take down policy
If you believe that this document breaches copyright please contact us at vbn@aub.aau.dk providing details, and we will remove access to the work immediately and investigate your claim.

Downloaded from vbn.aau.dk on: April 28, 2024

Check for updates

NANO · MICRO small
www.small-journal.com

Amorphous Materials for Lithium-Ion and Post-Lithium-Ion Batteries

*Junwei Ding, Dongfang Ji, Yuanzheng Yue, and Morten M. Smedskjaer**

Lithium-ion and post-lithium-ion batteries are important components for building sustainable energy systems. They usually consist of a cathode, an anode, an electrolyte, and a separator. Recently, the use of solid-state materials as electrolytes has received extensive attention. The solid-state electrolyte materials (as well as the electrode materials) have traditionally been overwhelmingly crystalline materials, but amorphous (disordered) materials are gradually emerging as important alternatives because they can increase the number of ion storage sites and diffusion channels, enhance solid-state ion diffusion, tolerate more severe volume changes, and improve reaction activity. To develop superior amorphous battery materials, researchers have conducted a variety of experiments and theoretical simulations. This review highlights the recent advances in using amorphous materials (AMs) for fabricating lithium-ion and post-lithium-ion batteries, focusing on the correlation between material structure and properties (e.g., electrochemical, mechanical, chemical, and thermal ones). We review both the conventional and the emerging characterization methods for analyzing AMs and present the roles of disorder in influencing the performances of various batteries such as those based on lithium, sodium, potassium, and zinc. Finally, we describe the challenges and perspectives for commercializing rechargeable AMs-based batteries.

1. Introduction

Enabling effective storage of the generated electric energy from renewable energy sources is the key to improve the energy utilization efficiency. An efficient storage strategy is needed to achieve "peak-shaving and valley-filling" grid-connected power generation, especially for intermittent energy sources such as wind and solar energies. Among different energy storage strategies, lithium-ion batteries (LIBs) and post-lithium-ion batteries are among the most promising ones. As a typical representative, LIBs are already widely applied, e.g., in mobile electronic products and electric vehicles.[1] Graphite has traditionally been used as the anode material in traditional LIBs, with a theoretical capacity of 372 mAh g^{-1}.[2] There are now enhanced LIBs available with high energy density using silicon anodes (theoretical capacity of 3579 mAh g^{-1}).[3] The ultimate goal is to use lithium metal (Li) anode with high theoretical capacity of 3860 mAh g^{-1}, which is the most promising one used in the so-called lithium–metal batteries (LMBs).[4] Moreover, traditional LIBs use liquid organic electrolytes, which have potential safety hazards that can be prevented through the use of solid electrolytes.[5] Unfortunately, the source of lithium in the earth's crust is limited and the lithium distribution is very nonuniform, resulting in very high price of lithium, which is only expected to increase in the future.[6] Fortunately, two other alkali metals, namely sodium (Na) and potassium (K), have abundant reserves and sodium-based and potassium-based batteries thus have good application prospects, especially for large-scale energy storage and low-speed electric vehicles.[7] Compared with monovalent lithium-, sodium-, and potassium-ions, divalent magnesium-, zinc-, and calcium-ions as well as trivalent aluminum-ions have the advantage of higher ion charge density, but lower ionic conductivity.[8] Especially for zinc-based batteries, the application of aqueous electrolytes offers intrinsically high safety and good application prospects in the field of large-scale energy storage. Meanwhile, batteries with nonmetallic charge carriers, such as hydrogen- and ammonium-ion (NH_4^+) batteries, have high power densities.[9]

Crystalline materials are typically used for fabricating cathodes, anodes, and solid electrolytes for batteries. Recently, disordered materials are emerging with the potential to enhance energy and/or power densities of batteries. This is highlighted by several recent advances. For instance, the Li-rich layer oxides with cation-disordered structures were utilized as cathode materials in LIBs with high electrochemical performances.[10] Note that these oxides are crystalline materials but possess a

J. Ding, Y. Yue, M. M. Smedskjaer
Department of Chemistry and Bioscience
Aalborg University
Aalborg 9220, Denmark
E-mail: mos@bio.aau.dk
D. Ji
College of Food and Bioengineering
Zhengzhou University of Light Industry
Zhengzhou 450002, China

The ORCID identification number(s) for the author(s) of this article can be found under https://doi.org/10.1002/smll.202304270

© 2023 The Authors. Small published by Wiley-VCH GmbH. This is an open access article under the terms of the Creative Commons Attribution License, which permits use, distribution and reproduction in any medium, provided the original work is properly cited.

DOI: 10.1002/smll.202304270

high degree of occupational disorder. Additionally, amorphous lithium was employed as metal anode to improve the battery performance,[11] and amorphous carbon was used as anode material for SIBs.[6] Amorphous materials (AMs) feature long-range structural disorder, which can be important for achieving high-performance in batteries. AMs can be divided into two categories, i.e., melt-quenched glasses and not-melt-quenched disordered materials. Although both are isotropic and long-range disordered, only the former have a glass transition temperature (T_g).[12] According to their chemistry, the melt-quenched glasses can be further divided into nonmetallic inorganic,[13] organic,[14] metallic,[15] and metal–organic framework (MOF) systems.[16] To understand the role of AMs in high-performance batteries, it is crucial to accurately characterize and analyze the structure and properties of AMs. Generally, the structural analysis of AMs is a complicated task since it lacks the lattice periodicity of the crystalline structure. AMs exhibit short-range order, medium-range partial order, and long-range disorder. The structural model theory of AMs has not been fully established. Overall, order/disorder engineering can regulate the electrochemical-, mechanical-, chemical-, and thermal properties of batteries.[17]

A comprehensive critical analysis of the use of AMs for making lithium-ion and post-lithium-ion batteries is still missing, although some reviews have described the applications of AMs for different batteries. These published reviews cover amorphous carbon-based anodes,[6,18] amorphous $NaFePO_4$ cathodes and V_2O_5-TeO_2 glass anodes,[17a] amorphous metal oxide anode and cathode materials,[19] amorphous anode and cathode materials for SIBs,[17d] amorphous lithium thiophosphate and lithium oxynitride electrolytes for solid-state batteries,[17c] and glassy superionic conductors for solid-state batteries.[20] The present review focuses on the fundamental understanding of the structure–property relation of AMs in relation to their battery performances. We begin by introducing the fundamentals of AM science and technology. Following that, we categorize amorphous battery materials and describe the pertinent experimental and simulation techniques. We clarify the functions of AMs in batteries and highlight the advanced properties of AM-based batteries, especially concerning their electrochemistry, mechanics, chemistry, and thermal behaviors. Finally, we discuss the challenges and perspectives for the development of AM-based batteries.

2. General Properties and Preparation Methods of AMs

Crystalline and amorphous solid materials can be distinguished based on their atomic-scale structure. While the atomic positions in a crystal feature long-range order (i.e., translational periodicity), there is no long-range order in amorphous solid materials. On the other hand, both crystalline and amorphous solids generally exhibit short-range order, and amorphous solid materials also have exhibit partial medium-range order. The amorphous solid state is an important subject in the condensed matter science.[21] The bonding types in amorphous solids can be divided into covalent (e.g., silica), metallic (e.g., alloys), ionic (e.g., thiophosphate), and coordination bonds (e.g., metal–organic frameworks). The short-range order of AMs results in the band-like structure of electron energy states.[22] Furthermore, the difference in the physical properties, such as density, mechanical, and thermal properties, between AMs and their crystalline counterparts depends on the chemical bond type and material composition as well as on preparation routes of AMs.

The general preparation methods of AMs can be summarized as follows: 1) high-energy ball milling; 2) melt-quenching; 3) physical and chemical vapor deposition; 4) irradiation; 5) chemical methods (e.g., hydrogenation and chemical plating); 6) large supercooling of pure melt (e.g., droplet emulsion method and flux method); 7) high pressure, and so on.[23] In general, almost all AMs can be obtained by high-energy ball milling. Since the high-energy ball milling method can be applied at a large scale, it has certain advantages, e.g., low energy consumption and low production cost, for producing AM battery materials. The melt-quenching method can be scaled up, but it necessitates high temperatures. Therefore, it is crucial to choose suitable material composition to reduce the melting point.

3. AM-Based Batteries

3.1. Classification and Application of AMs

Recently, the use of AMs to construct high-performance batteries has received increasing attention. Replacing AMs for the traditional crystalline battery materials will affect the electrochemical, mechanical, chemical, and thermal properties of lithium-ion and post-lithium-ion batteries (**Figure 1**). There are various glass systems including nonmetallic inorganic (oxides, sulfides, phosphate, silicate, etc.),[13] organic,[14] metallic,[15] and MOF glasses (such as zeolitic imidazolate frameworks (ZIFs)-62/4).[16] Among glass materials, oxide and sulfide glasses have been most studied as candidates for solid-state electrolytes.[24] Organic glasses such as polymers can also be used in solid-state electrolytes due to their good processability, structural designability, and flexibility.[25] Moreover, as a newly discovered glass family, MOF glasses have displayed attractive applications as both electrode materials and solid-state electrolytes for lithium batteries.[26] Nonglassy AM consists of inorganic, organic, and hybrid types. Most crystalline inorganic materials can be transformed into the amorphous state by mechanical ball milling. As a promising electrode material, amorphous carbon plays an important role in many types of batteries.[6,18] It is thus clear that different types of AMs can be used to obtain batteries with different characteristics.

3.2. Characterizations of AMs and Their Working Mechanism in Batteries

Figure 2 presents an overview of both experimental and theoretical simulation methods. The former ones involve X-ray scattering (XS) consisting of elastic and inelastic scattering techniques,[27] neutron scattering, nuclear magnetic resonance (NMR), Fourier transform infrared spectroscopy (FTIR), Raman spectroscopy, etc. In the case of crystalline materials, X-ray diffraction and transmission electron microscopy (TEM) can be used to understand their periodic atomic structure, but in contrast, only give limited structural information about AMs.[17d] Raman and FTIR can detect the vibration modes of different chemical bonds in

© 2023 The Authors. Small published by Wiley-VCH GmbH

16136829, 0, Downloaded from https://onlinelibrary.wiley.com/doi/10.1002/smll.202304270 by Aalborg University Library, Wiley Online Library on [06/12/2023]. See the Terms and Conditions (https://onlinelibrary.wiley.com/terms-and-conditions) on Wiley Online Library for rules of use; OA articles are governed by the applicable Creative Commons License

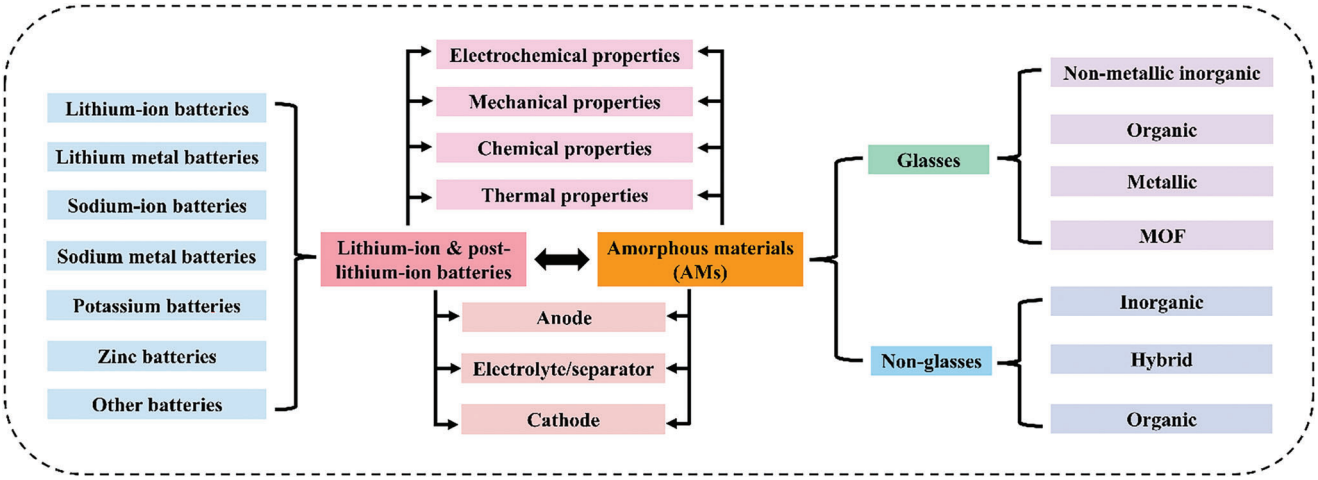

Figure 1. Schematic diagram of glass and nonglass AMs for lithium-ion and post-lithium-ion batteries.

AMs, while NMR,[28] X-ray absorption spectroscopy (XAS),[29] and X-ray and neutron scattering[30] can give structure information on different length scales. Moreover, operando characterization with these methods is critical to understand the evolution of AMs during the electrochemical process and thus the internal working mechanism. For example, the ionic conductivity of a bulk glassy electrolyte may change when the same glassy electrolyte is confined between porous electrode structures. Currently, there are relatively few operando studies involving amorphous battery materials.[31]

The results of NMR, XAS, and X-ray and neutron scattering can be mutually compared with theoretical calculations, including classical molecular dynamics (MD), ab initio molecular dynamics (AIMD), and finite element analysis. The electrochemical, mechanical, chemical, and thermal properties of AMs can be calculated based on the obtained amorphous structure model. Theoretical simulations are especially an important tool to explain the working mechanism of AMs in the case where experimental tests cannot be effectively implemented, such as interfacial interactions in batteries.[20] Since the different battery components need to have compatible interfaces to work stably, further in-depth understanding of the interaction at the interfaces is needed. Therefore, establishing machine learning (ML) potentials to simulate full component nanosize batteries is one of the very promising directions for understanding the interface ion/electron transport under an electric field. Although AIMD may offer the structural accuracy for describing the interface behavior, it is computationally too expensive to construct nanobatteries as it has been done with classical MD.[32] To this end, ML-based force fields could offer the good compromise between structural accuracy and reasonable computation to allow the construction of realistic models of simulated nanobatteries.

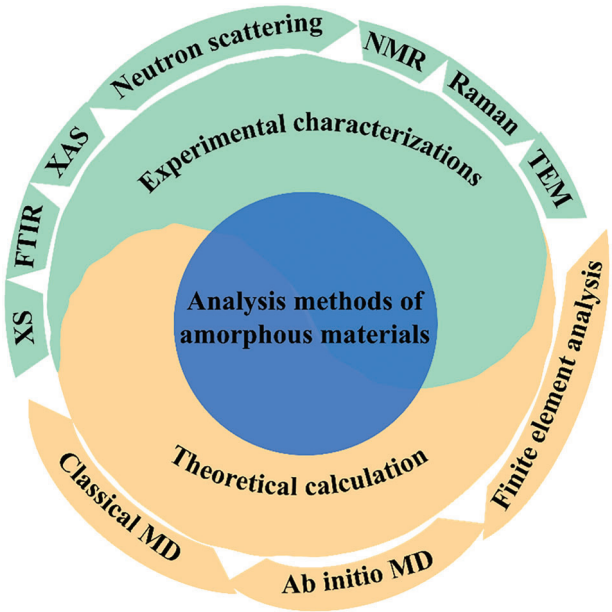

Figure 2. Overview of different analysis methods for amorphous battery materials via experimental techniques and theoretical calculations.

3.3. Four Key Properties of AMs for fabricating Batteries

Generally, the influence of AMs on battery performances can be divided into four aspects: electrochemical, mechanical, chemical, and thermal properties. Among them, the chemical properties (e.g., ion storage and transfer kinetics, structure evolution during ion storage, and interface stability during contact) can be determined by the experimental and simulation methods mentioned above. The thermal performance can be analyzed and compared directly through the thermal conductivity and the thermal stability. Indeed, the thermal runaway behavior of rechargeable batteries under extreme conditions is closely related to the chemical and thermal properties of the battery components. The flame retardancy or the high thermal conductivity of AMs (e.g., the abnormally higher thermal conductivity of MOF glass compared to its counterpart-MOF crystals[33]) can be used to suppress the thermal runaway and/or increase the thermal stability of batteries.[34] Regarding the mechanical properties (**Figure 3**), batteries with different physical shapes (such as coin-cell and pouch-cell) have different requirements for the mechanical performances of each battery component.[35] Especially

© 2023 The Authors. Small published by Wiley-VCH GmbH

16136829, 0, Downloaded from https://onlinelibrary.wiley.com/doi/10.1002/smll.202304270 by Aalborg University Library, Wiley Online Library on [06/12/2023]. See the Terms and Conditions (https://onlinelibrary.wiley.com/terms-and-conditions) on Wiley Online Library for rules of use; OA articles are governed by the applicable Creative Commons License

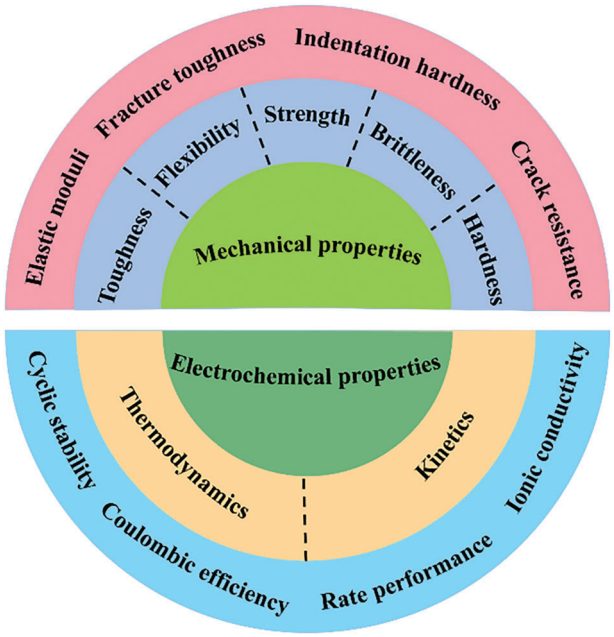

Figure 3. Different parameters of mechanical and electrochemical properties of AMs for different batteries.

for solid-state batteries, the analysis and tuning of mechanical properties of battery components are very important.[36] The electrochemical properties are central to the commercial use of batteries, and the thermodynamic and kinetic parameters of AMs must meet the requirements for different battery components regarding capacity, ionic conductivity, rate performance, and so on. Considering that the battery is composed of different components with different requirements for mechanical, thermal, and electrochemical performances, it is insufficient to analyze only a single performance index. That is, the coupling relationships between the different performances need to be clarified.

3.4. Lithium-Based Batteries

The layered oxides and graphite are usually utilized as cathodes and anodes, respectively, for commercial LIBs, where lithium ions undergo reversible intercalation and deintercalation. With the ever-increasing demand for high energy and power densities, AMs are being introduced into different components of LIBs,[37] to enhance the electrochemical, mechanical, chemical, and thermal performances.[24a,38]

3.4.1. Glass Anodes for Lithium Batteries

Inspiringly, the first melt-quenched MOF glass anode, i.e., cobalt-ZIF-62 glass anode, has recently been developed for LIBs (**Figure 4**a).[26a] The obtained anode delivers a high capacity of 306 mAh g^{-1} at the current density of 2 A g^{-1} as well as higher cycle stability and rate performance compared with both the crystalline and the ball-milling-derived amorphous cobalt-ZIF-62 anodes. When 10 wt.% nanosilicon is introduced into cobalt-ZIF-62 glass, the amorphous composite anode can be made, and its capacity can even reach 650 mAh g^{-1} at 1 A g^{-1}.[26c] Density functional theory (DFT) calculations reveal that the aromatic rings in imidazoles and benzimidazoles are lithium-ion binding sites (Figure 4b–d). The barrier for diffusion of lithium-ions from one organic ligand to another is also found to be low (Figure 4e). Based on the experimental and simulation analyses, it is found that the distortion and partial breakage of Co—N coordination bonds in the MOF glass anode increase the active sites accessible to lithium ions during the discharging/charging cycling. Figure 4f,g shows the electrochemical performances of a melt-quenched chalcogenide glass anode ($Ge_2Sb_2Se_5$) with the capacity of 626 mAh g^{-1} and good cycling stability via lithiation mechanism of Se, Sb, and Ge.[39] Moreover, by incorporating Li_2O into V_2O_5-TeO_2 glasses, the structure and battery performances can be altered (Figure 4h).[40] In this work, a DFT model was constructed to calculate the diffusion barrier of Li atoms in crystal electrodes and this model also applies to the amorphous electrodes. Based on this model, the lithium diffusion barriers in V_2O_5 and VO_2 crystals are found to be 0.49 and 0.16 eV, respectively, revealing that the Li^+ diffusion impedance becomes lower owing to the contribution of valence state change and chain scission (Figure 4i). The V—O electrostatic potential confirms that VO_2 can reconstruct a smooth electrostatic atmosphere and lower the lithium-ion diffusion barrier (Figure 4j). Based on various analyses, it is concluded that adding Li_2O may increase ion diffusivity, electron conductivity, and stability of ion environment, thereby resulting in the enhanced battery performances.

Silicon is a promising anode material for LIBs because of its high theoretical capacity. To this end, a self-supporting anode consisting of silicon oxycarbide (SiOC) glass and reduced graphene oxide (rGO) substrate has been constructed.[41] It is confirmed that the large size rGO sheets serve as flexible and electronic host while the nanodomain SiOC glass serves as the main active material with chemical and thermodynamic stability to simultaneously achieve high electrochemical and mechanical performances (**Figure 5**a). The 60SiOC sample has a tensile strength of ≈2.7 MPa with a strain of 1.1% (Figure 5b,c). The obtained electrode delivers a capacity of ≈588 mAh g^{-1} after 1000 cycles and shows no obvious mechanical failure. Other glass materials have also been reported to serve as anodes of LIBs, including CoO-GeO_2-Li_2O-B_2O_3,[42] Li_2O-B_2O_3-GeO_2,[43] MoO_3-TeO_2,[44] Li_3PS_4,[45] TeO_2-V_2O_5-P_2O_5,[46] tin fluorophosphate ($NH_4H_2PO_4$-SnO-SnF_2),[47] V_2O_5-P_2O_5,[48] TeO_2-V_2O_5-Al_2O_3,[49] Sn-based glass-graphite,[50] SiO_x-C,[51] etc. The corresponding numerical comparison of their electrochemical properties are summarized in Table S1 in the Supporting Information.

The above-mentioned studies demonstrate that glass-based LIB anode materials have achieved remarkable development. However, there are still challenges in terms of obtaining superior electrochemical properties, including capacity, rate performance, and cycling stability. To further develop glass anodes with real commercial application value, the development of composite glass anodes seems especially attractive as it can combine the advantages of different glass anodes, but to our knowledge, no composite glass anodes have yet been reported. We note that when preparing composite glass anodes, the electrochemical compatibility of each component needs to be considered,

© 2023 The Authors. Small published by Wiley-VCH GmbH

16136829, 0, Downloaded from https://onlinelibrary.wiley.com/doi/10.1002/smll.202304270 by Aalborg University Library, Wiley Online Library on [06/12/2023]. See the Terms and Conditions (https://onlinelibrary.wiley.com/terms-and-conditions) on Wiley Online Library for rules of use; OA articles are governed by the applicable Creative Commons License

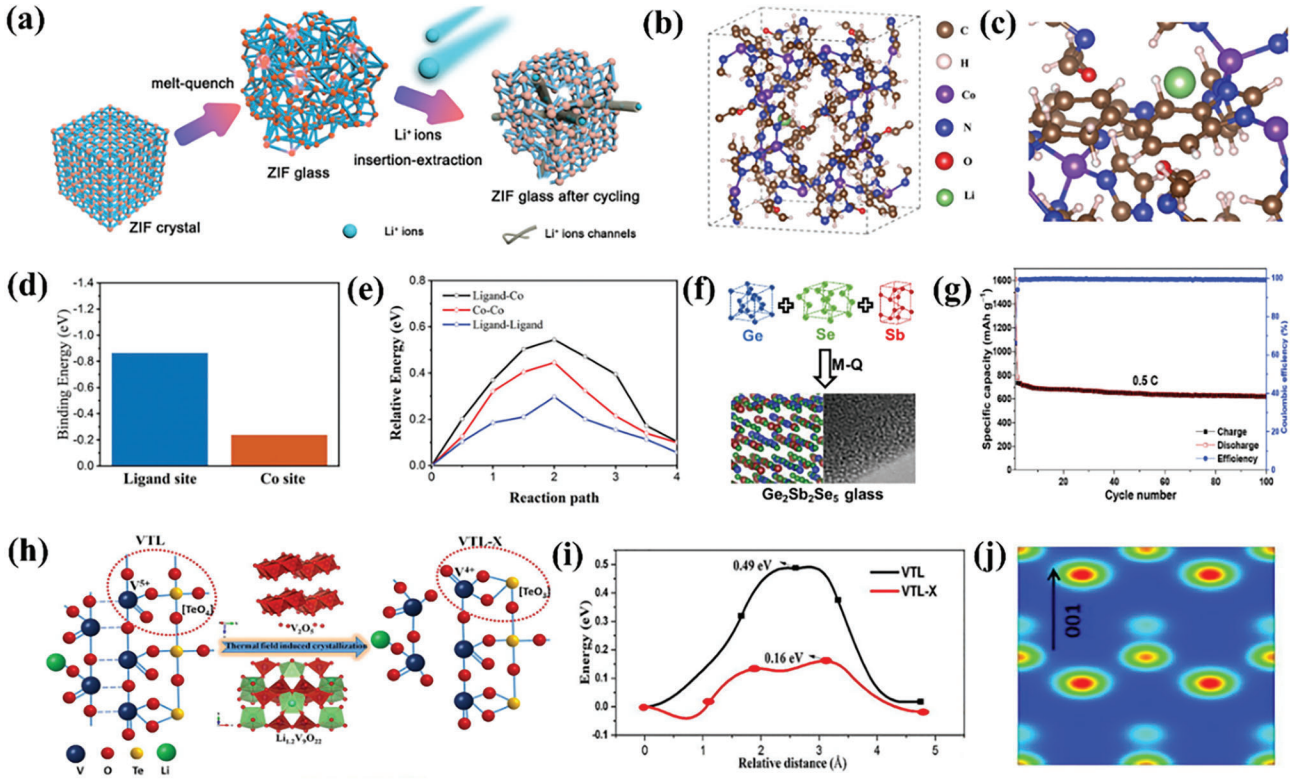

Figure 4. a) Structural evolution of cobalt ZIF-62 glass anode upon cycling. b) Simulated cobalt ZIF-62 crystal and lithium-ion binding sites. c) Enlarged view of lithium binding site in panel (b). d) Binding energy of organic ligands and metal sites. e) Relative energy barriers of three diffusion approaches. f) Preparation of glassy $Ge_2Sb_2Se_5$ via melt-quenching. g) Cyclic performance at 0.5 C of glassy $Ge_2Sb_2Se_5$. h) The structural change of V_2O_5-TeO_2-Li_2O during thermal field treatment. i) Lithium-ion energy barriers and j) cross-sectional electrostatic potential. (a–e) were reproduced with permission.[26a] Copyright 2022, Wiley-VCH GmbH. (f) and (g) were reproduced with permission.[39] Copyright 2020, Elsevier. (h–j) were reproduced with permission.[40] Copyright 2022, Elsevier.

especially to match the working voltage range. Furthermore, obtaining a uniform composite glass anode in nanometer size requires the development of new preparation techniques.

3.4.2. Glass Electrolytes for Lithium Batteries

In addition to being used as anode materials, glasses can also serve as electrolyte materials for lithium batteries. For example, a zinc-based ZIF-4 glass has been used to construct a quasi-solid-state electrolyte (Figure 5d,e).[26b] With 0.12 wt.% lithium and 19.4 wt.% solvent, the obtained electrolyte delivers the high ion conductivity (0.161 mS cm^{-1} (30 °C) and 5.96 × 10^{-3} mS cm^{-1} (−56.6 °C). Since there are no grain boundaries and isotropic structure in ZIF-4 glass particles, the enhanced ion diffusion enables homogeneous lithium plating/stripping. Thus, MOF glasses are promising quasi-solid-state electrolytes for practical solid-state batteries owing to their structural anisotropy, no grain boundary inside the bulk phase, adjustable pore structure, and designable metal and organic ligands. The Li_2S-P_2S_5 glass system has been extensively studied as solid electrolytes.[55] Unfortunately, the mechanical measurement on sulfide electrolytes is challenging owing to their humidity and oxygen sensitivity. Based on the mineral oil protection indentation test, the indentation fracture toughness K_{Ic} of a glassy $70Li_2S$-$30P_2S_5$ solid electrolyte was found to be 0.23 ± 0.04 MPa $m^{1/2}$ via crack length analysis (Figure 5f).[52] K_{Ic} remains almost stable over the test period (Figure 5g), confirming that the sample surface is stable via the protection of mineral oil. Very recently, via classification-based ML analysis, the impact of anion clusters ($P_2S_6^{4-}$, $P_2S_7^{4-}$, and PS_4^{3-}) on lithium conduction in glassy thiophosphate electrolytes has been uncovered. The lithium ions with high mobility are mainly found around PS_4^{3-} units, while the low mobility ions are found around $P_2S_6^{4-}$ units.[56] Remarkably, superior Li_2S-P_2S_5-B_2S_3 electrolytes have been developed via a ball-milling and then melt-quenching strategy.[57] The structural and chemical heterogeneities in these materials were found to be the main origin of the continual interphase evolution. The resulted "multilayer mosaic like" interphase suppresses Li dendrite growth, and hence, extends the lifetime of all-solid-state LIBs. In addition, the preparation technique of these solid electrolytes is feasible for scale-up production. The quaternary lithium oxythioborate halide glasses (Li_2S-B_2S_3-SiO_2-LiI) have also been found to exhibit high ion conductivity up to 2 mS cm^{-1} and obviously reduced H_2S evolution property (confirming the enhanced structure stability).[53] ^{11}B and ^{29}Si NMR studies of these glasses confirm that the local glass structure facilitates fast ion diffusion with various tetrahedral silicon as well as trigonal/tetrahedral boron species (Figure 5h,i). Lithium plating/stripping can work with very small polarization voltage at 0.1 mA cm^{-2}.

© 2023 The Authors. Small published by Wiley-VCH GmbH

16136829, 0, Downloaded from https://onlinelibrary.wiley.com/doi/10.1002/smll.202304270 by Aalborg University Library, Wiley Online Library on [06/12/2023]. See the Terms and Conditions (https://onlinelibrary.wiley.com/terms-and-conditions) on Wiley Online Library for rules of use; OA articles are governed by the applicable Creative Commons License

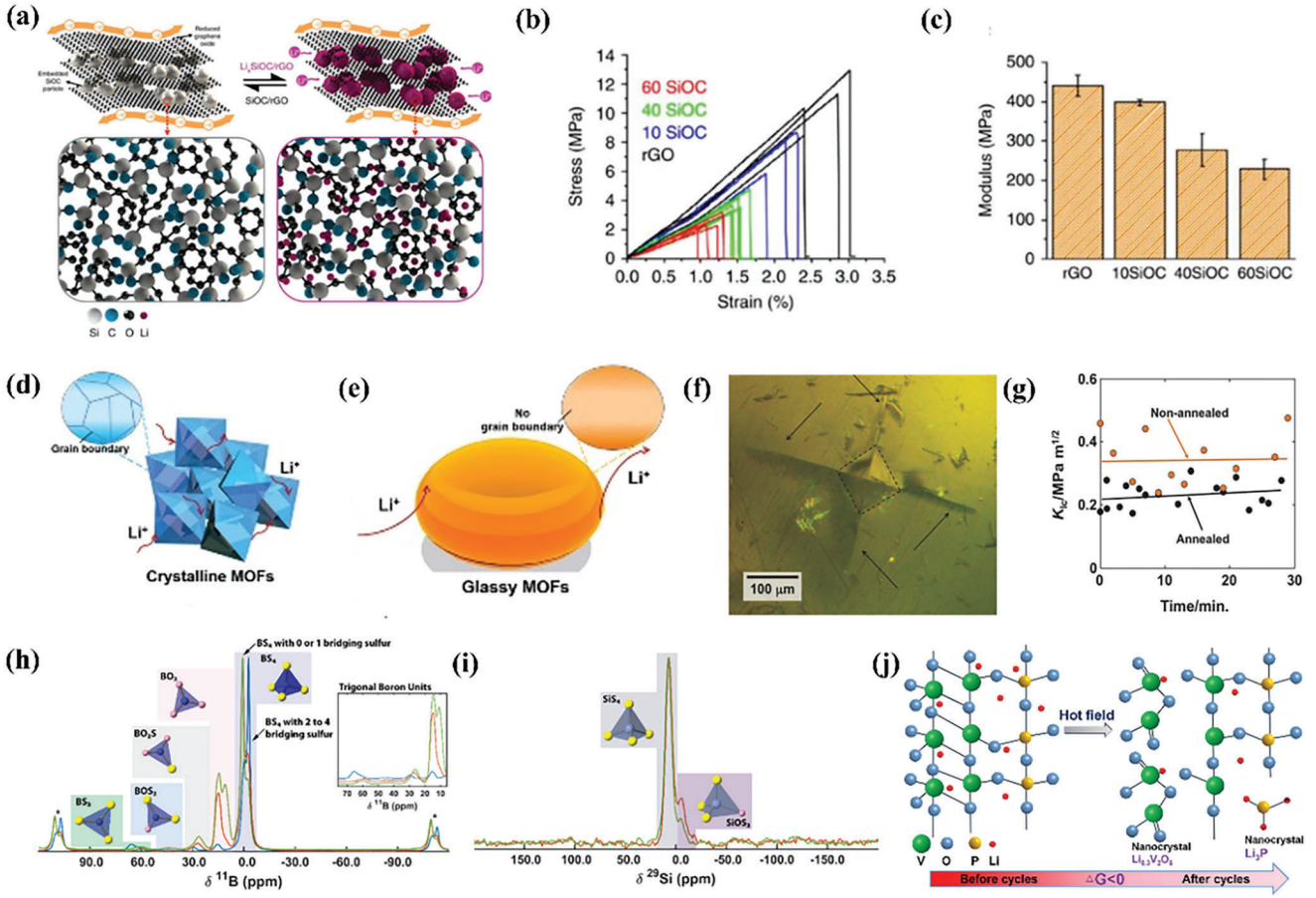

Figure 5. a) Schematic representation of the mechanism of lithiation and delithiation process for silicon oxycarbide (SiOC) glass particles. b) Stress versus strain curves. c) Modulus values. (a–c) were reproduced with permission.[41] Copyright 2016, Springer Nature. d) Lithium-ion diffusion in crystalline zinc ZIF-4. e) Lithium-ion conduction in zinc ZIF-4 glass. (d) and (e) were reproduced with permission.[26b] Copyright 2021, Wiley-VCH GmbH. f) Fracture resulting from Vickers indentation on glassy Li_2S-P_2S_5. g) Fracture toughness of annealed and nonannealed specimens. (f) and (g) were reproduced with permission.[52] Copyright 2017, Wiley-VCH GmbH. h) ^{11}B and i) ^{29}Si magic-angle spinning (MAS) NMR of $LiB_{0.5}Si_xO_{2x}Sl_{0.5}$ with $x = 0$, 0.25, and 0.5, respectively. (h) and (i) were reproduced with permission.[53] Copyright 2020, Wiley-VCH GmbH. j) Schematic of the order and disorder transformation of V_2O_5-Li_3PO_4 glass. Reproduced with permission.[54] Copyright 2021, Elsevier.

Additionally, a new Li_3BN_2 glass electrolyte with an ionic conductivity of 0.013 mS cm^{-1} at 25 °C has been reported.[58]

In addition to the request for high ionic conductivity, the electrolytes must have orbital energy levels that match those of the anodes and cathodes. Therefore, the development of glassy electrolytes necessitates careful consideration of the characteristics of both the anode and cathode materials. This involves the selection of glass systems with suitable composition, glass-forming capability, chemical stability, electrochemical properties, and mechanical properties. In view of the diversity of glass systems, applying machine learning based techniques for materials discovery and inverse design is a promising research direction.[59]

3.4.3. Glass Cathodes for Lithium Batteries

Cathode materials not only need to have a combination of high ionic and electronic conductivities, but also a sufficiently high electrode potential. To this end, applying glass defect engineering, the disorder–order change cathode of LIBs can be achieved.[54] That is, battery cycling can cause the disorder–order transition of V_2O_5-Li_3PO_4 glass, resulting in the crystal formation of Li_3P and $Li_{0.3}V_2O_5$. The results suggest that the long-cycle electric fields have the same effect on glass cathode compared with the thermal field induction process (Figure 5j).[54] Meanwhile, MoO_3-P_2O_5, FeF_3-V_2O_5, and Li_2O-V_2O_5-B_2O_3 glasses can also be used as the cathode materials for LIBs.[60]

These above analyses indicate the performances of developed glass cathode materials remain limited. This is because traditional methods are generally based on time-consuming trial-and-error. The most critical property for the cathode material is to have sufficiently high electrode potential. The special requirements of the cathode determine the need to find materials with suitable chemical composition and high glass-forming ability. To this end, we propose that artificial intelligence methods such as applying ML to screen and develop new cathodes as it enables rapid screening of promising candidates. Moreover,

© 2023 The Authors. Small published by Wiley-VCH GmbH

16136829, 0, Downloaded from https://onlinelibrary.wiley.com/doi/10.1002/smll.202304270 by Aalborg University Library, Wiley Online Library on [06/12/2023]. See the Terms and Conditions (https://onlinelibrary.wiley.com/terms-and-conditions) on Wiley Online Library for rules of use; OA articles are governed by the applicable Creative Commons License

for multicomponent glass systems, the cycle of developing new high-performance glass cathodes can be shortened. However, there are few available ML interatomic potentials for amorphous materials.[20] Thus, the long-time and large spatial scale simulations with ML potentials for the glassy cathode are promising avenues for further studies.

3.4.4. Nonglassy AMs for Lithium Batteries

Nonglassy AMs can also be used for fabricating anodes, electrolytes, and cathodes for lithium batteries (see list of materials in Table S2, Supporting Information). As is known, the amorphous carbon-based materials with various morphologies and structures have been developed and investigated.[18] Amorphous lithium metal features higher electrochemical reversibility compared with the crystalline Li counterpart.[11] It has been found that lithium clusters with more than 700 lithium atoms can transform into the bcc lattice structure, whereas lithium clusters with fewer than 700 lithium atoms remain in their disordered structure. The amorphous nature (i.e., without ordered nanostructure and grain boundary) of the lithium metal facilitates the omnibearing growth of small lithium grains into large ones, resulting in the dense and uniform lithium formation (not the lithium dendrite), which is beneficial to the practical application of lithium metal anodes. In addition, amorphous SiO_2-TiO_2 affects the lithium plating behavior to achieve uniform deposition.[61] In 1997, amorphous tin-based oxides were reported as high-capacity lithium storage materials.[62] In the following years, various amorphous oxides for lithium storage were reported.[63] Among these, iron-based oxides are promising for commercial applications because of their abundant reserves.[64] For example, amorphous Fe_2O_3 exhibits high cycling stability and rate performance as well as low voltage hysteresis.[65] A high capacity of ≈1600 mAh g^{-1} is observed at 1 A g^{-1} after 500 cycles. According to DFT results, amorphous Fe_2O_3 exhibits that the Gibbs free energy change (ΔG) for the reaction of lithium ions with the hosting materials is 0.27 eV lower than that of its crystalline counterpart (**Figure 6**a), confirming the enhanced reversibility during cycling. Furthermore, the isotropy and lack of grain boundaries is beneficial to sustaining high strain during lithium intercalation, and hence, to inhibiting the structure collapse during a long cycling process. Amorphous iron selenite (FeSeO) has also been reported as anode material (Figure 6b). Based on a low temperature preparation method, the obtained samples show the high capacity of 617 mAh g^{-1} at 30 A g^{-1} and long cycle stability up to 1800 cycles.[66] Many other types of amorphous materials for LIB anodes have also been developed, e.g., amorphous silicon (Si),[67] molybdenum dioxide,[68] $MnSiO_3$,[69] P_4SSe_2,[70] LiV_3O_x,[71] germanium (Ge),[72] SnO_2,[73] TiO_x/Si/TiO_x,[74] V_2O_3,[75] ZnO,[76] boron (B),[77] organic polymer,[78] and red phosphorus (P)[79] anodes of LIBs. Additionally, we note that amorphous TiO_2 shell can be used as the elastic buffering layer to enhance the stability of the silicon nanoparticle anode.[80]

Overall, we find that the use of nonglassy AMs in anodes of LIBs has been extensively studied. Commercialization requires the use of pouch-type instead of coin-type batteries, i.e., more studies should focus on the development of pouch cells to evaluate the practical index parameters of such AMs. In addition, there is a need to analyze the price, raw material, and degree of recycling of the developed materials for large-scale production and replacement of currently commercialized components of LIBs. Compared with glassy anodes with limited types and fabrication techniques, there are enough available nonglassy anodes with different characteristics, which can be prepared via various methods.

Amorphous Li_3BO_3 with high deformability was demonstrated to be a potential solid electrolyte for all-solid-state LIBs. The high deformability is important for obtaining superior electrolyte/electrolyte homointerfaces and electrode/electrolyte heterointerfaces even without a firing process.[85] Amorphous silicon nitride (Si_3N_4) has been used as a functional filler for solid polymer electrolytes, resulting in excellent battery performance (Figure 6c).[81] This is because its high dielectric constant facilitates the uniform lithium plating via a screening effect. The product $LiSi_2N_3$ formed during the reduction reaction between lithium and Si_3N_4 exhibits a fast lithium-ion diffusion ability. Furthermore, the high thermal stability of Si_3N_4 enhances the antiflammability of Si_3N_4 based polymer solid-state electrolyte. In another polymer-based system, a novel crosslinked polyether with silyl end-capping has been synthesized as an amorphous electrolyte. It features high ionic conductivity (up to ≈0.36 mS cm^{-1} at room temperature), high ion transference number (≈0.65), stable electrochemical window (5.0 V vs. Li^+/Li), and excellent compatibility to the electrode (Figure 6d).[25] Considering that both AMs and polymers have their own network structures, the development of composite electrolytes based on AMs and polymers is a very promising direction. Especially, future studies should focus on MOF glass and polymer based composite electrolytes considering that the adjustable and similar characteristic of organic ligands in MOFs and the repeating unit in polymers. Moreover, the resulting composite electrolyte can feature excellent machinability and electrochemical activity owing to its ability to combine the excellent processability of polymers with the high electrochemical activity of amorphous electrolytes.

The amorphous but nonglassy iron fluorosulfate (a-$LiFeSO_4F$) cathode displays high capacity and unexpectedly high reversibility via the synergetic intercalation and conversion mechanism.[86] The intercalation reaction is related to the Fe^{2+}/Fe^{3+} redox ratio caused by the reaction between a-$LiFe^{2+}SO_4F$ and $Fe^{3+}SO_4F$, while the conversion reaction is related to the Fe^0/Fe^{2+} ratio determined by Fe^0, $LiSO_3F$, Li_2O, and a-$LiFe^{2+}SO_4F$. a-$LiFeSO_4F$ has a capacity of >250 mAh g^{-1} at 1000 mA g^{-1}, indicating good rate performance. Alternatively, amorphous chromium-vanadium oxide,[87] iron vanadate ($FeVO_4$),[88] $LiCoO_2$-Li_2SO_4,[89] iron-based oxyfluorides,[90] TiS_4,[91] and vanadium-phosphorus-lithium[92] can also be applied as cathode materials for LIBs. These studies show that developing amorphous cathode materials with both intercalation/extraction and conversion mechanisms is a very promising strategy to obtain both high capacity and long cycle stability. Notably, most cathodes suffer from degradation.[93] Surface coating is a promising method to suppress the degradation.[94] To this end, based on high-throughput simulations, researchers have reported seven promising amorphous coating candidates, i.e., LiB_3O_5, $LiPO_3$, $Li_3B_{11}O_{18}$, $LiAlSiO_4$, $LiZr_2(PO_4)_3$, $LiSb_3O_8$, and $LiTaSiO_5$, which exhibit high thermodynamic and electrochemical stability as well as the low chemical reactivity with electrolytes (Figure 6e).[82] Lithium-sulfur and lithium-oxygen

© 2023 The Authors. Small published by Wiley-VCH GmbH

16136829, 0, Downloaded from https://onlinelibrary.wiley.com/doi/10.1002/smll.202304270 by Aalborg University Library, Wiley Online Library on [06/12/2023]. See the Terms and Conditions (https://onlinelibrary.wiley.com/terms-and-conditions) on Wiley Online Library for rules of use; OA articles are governed by the applicable Creative Commons License

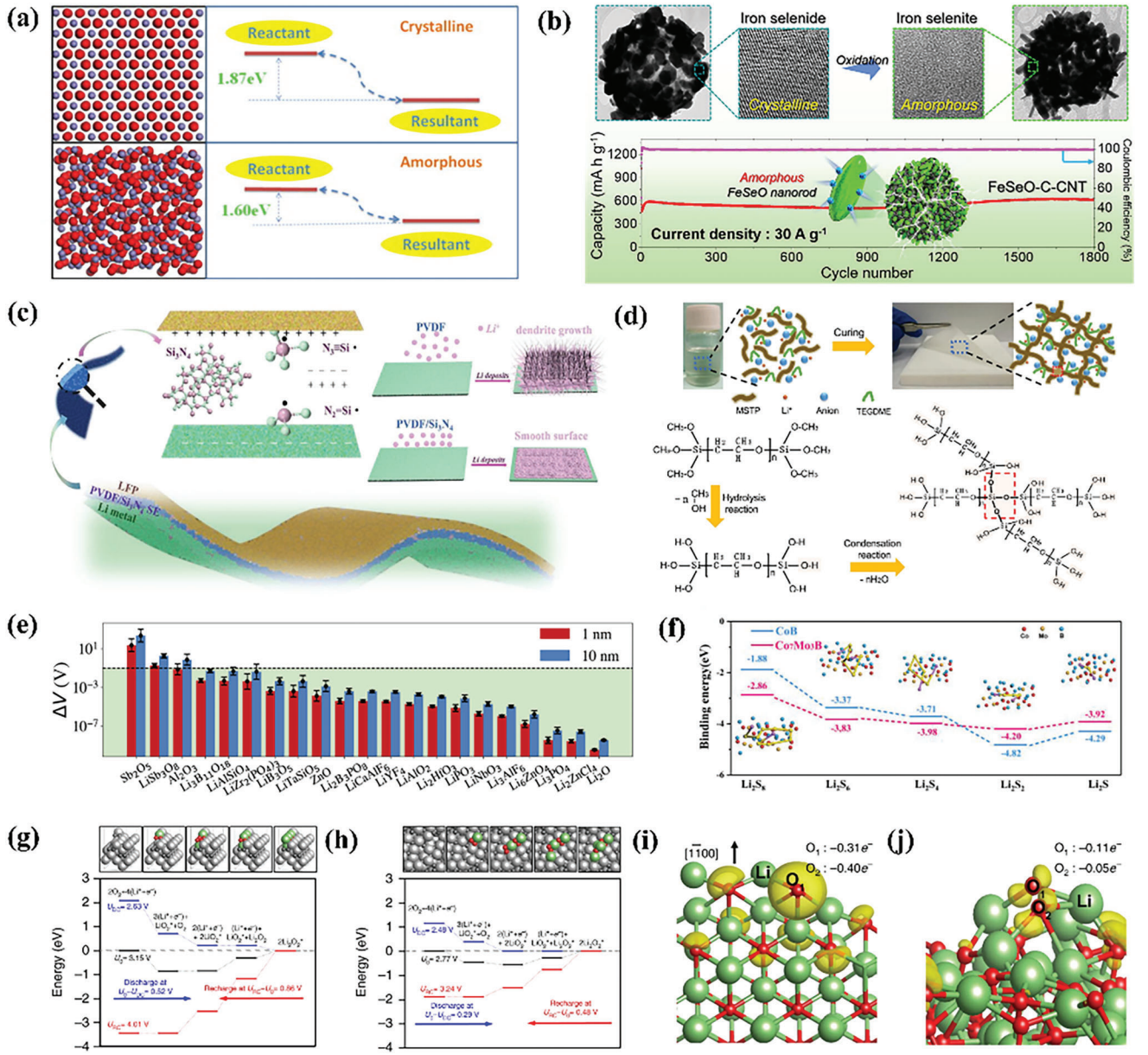

Figure 6. a) Energy difference between reactant and the corresponding final product for crystalline α-Fe_2O_3 and amorphous Fe_2O_3. Reproduced with permission.[65] Copyright 2014, Elsevier. b) Amorphous iron selenite with high-rate performance and excellent cyclic stability. Reproduced with permission.[66] Copyright 2020, Elsevier. c) Schematic of lithium plating with and without amorphous Si_3N_4 based electrolytes. Reproduced with permission.[81] Copyright 2022, Elsevier. d) Modified silyl-terminated polyether, showing images before and after polymerization and the related molecular structures. Reproduced with permission.[25] Copyright 2017, Elsevier. e) Calculated overpotentials for various cathode coatings. Reproduced with permission.[82] Copyright 2022, The Royal Chemical Society. f) Relative free energy on CoB and Co_7Mo_3B interfaces during the reduction process from S_8 to Li_2S. Reproduced with permission.[83] Copyright 2022, Wiley-VCH GmbH. g) Calculated free energy of crystalline Li_2O_2. h) Calculated free energy of amorphous Li_2O_2. i,j) Electron density variation upon the initial LiO_2 adsorption on the surfaces of crystalline and amorphous Li_2O_2, respectively. (g–j) were reproduced with permission.[84] Copyright 2018, Springer Nature.

(air) batteries have ultrahigh theoretical energy densities of ≈2600 and 3000 Wh kg^{-1}, respectively. Interestingly, amorphous sulfur,[95] and lithium sulfide[96] can then directly be used as high-performance cathodes for lithium–sulfur batteries. An amorphous molybdenum doped cobalt boride (Co_7Mo_3B) was developed as the catalyst to accelerate sulfur cathode redox kinetics by finding the suitable binding energy between Co_7Mo_3B and long-chain lithium polysulfides as well as short-chain Li_2S_2/Li_2S (Figure 6f).[83] Amorphous cobalt phosphide,[97] Al_2O_3,[98] NiS_2,[99] MoS_3,[100] and TiO_2[101] are also proposed to enhance the reactivity of the sulfur cathode. In addition, an amorphous V_2O_5-modified separator can improve the sulfur cathode activity.[102] Similarly, by using amorphous lithium peroxide (Li_2O_2), high round-trip efficiency in lithium–oxygen batteries

© 2023 The Authors. Small published by Wiley-VCH GmbH

16136829, 0, Downloaded from https://onlinelibrary.wiley.com/doi/10.1002/smll.202304270 by Aalborg University Library, Wiley Online Library on [06/12/2023]. See the Terms and Conditions (https://onlinelibrary.wiley.com/terms-and-conditions) on Wiley Online Library for rules of use; OA articles are governed by the applicable Creative Commons License

can be achieved.[84] The overpotentials of oxygen evolution reaction (OER) for amorphous Li_2O_2 at the suitable binding site and crystal Li_2O_2 are 0.48 and 0.86 V, respectively. With the potential determining step of OER, the fundamental reason of the decreased overpotential of OER is the weak binding of $^*LiO_2$ on the amorphous Li_2O_2 surface. For oxygen reduction reaction (ORR), there is limited new coordination of $^*LiO_2$ on the amorphous surface (Figure 6g–j). The influence of the amorphous lattice structure on the potential determining step of OER is greater than that of ORR, resulting in more pronounced Li_2O_2 decomposition on the amorphous structure phase. Furthermore, applying amorphous LiO_2 as cathode for Li–oxygen battery can achieve low overpotential and high rate performance.[103] Similarly, amorphous TiO_{2-x} with oxygen-defect based cathode for the high-performance lithium–air battery can also be used.[104]

The above-mentioned studies indicate that applications of AMs as cathode surface coating, catalyst, cocatalyst, and active material in lithium batteries are promising. More types of AMs should be developed to meet the requirements of different cathodes. For cathode surface coating, AMs need to have good mechanical and chemical stability, enabling them to maintain structural integrity during electrochemical reactions at the cathode. Furthermore, good ionic conductivity is required to ensure the smooth progress of the cathode redox reaction. For catalysts and cocatalysts, AMs should have enough active sites, large specific surface area, and excellent structural stability to enable the active materials to react continuously and efficiently. AMs as active materials should exhibit both high ionic and electronic conductivity.

3.5. Sodium- and Potassium-Based Batteries

Considering the limited and nonuniform distribution of lithium resources, sodium and potassium with abundant reserves are alternative candidates for large-scale energy storage batteries. There has been an increasing interest in exploring AMs for use in sodium- and potassium-based batteries, as summarized in Tables S3–S5 in the Supporting Information.[24b,105]

3.5.1. Glass Materials for Sodium Batteries

First, it has been clearly demonstrated that glasses can serve as the anode materials of SIBs. For example, Na-Bi-Ge glass anode shows excellent electrochemical performances such as high rate and long cycle stability.[106] In addition, Na-Ge,[107] SnO-GeO_2-Sb_2O_3,[108] and tin-phosphate[109] glass anodes have been developed. Considering the larger size of sodium relative to lithium ions, glass anodes with more open volume for storage space need to be developed. To design a solid electrolyte with high electrochemical stability towards sodium metal, the glassy oxysulfide ($Na_3PS_{4-x}O_x$) with high critical current density was developed and tested (**Figure 7**a).[110] Using a pressure-applied sintering method at room temperature, the $Na_3PS_{4-x}O_x$ material was obtained, which exhibits a uniform glass structure with high mechanical strength due to the presence of bridging oxygens. The self-passivating solid electrolyte interphase is also a key for achieving stable reversible sodium plating/stripping. The $Na_3PS_{3.4}O_{0.6}$ glass has a homogeneous surface and bulk structure (Figure 7b,c) and is densified at a relatively lower pressure of 150 MPa (Figure 7d) compared with glassy Na_3PS_4 and heat-treated Na_3PS_4 (HT-Na_3PS_4). Two critical mechanical properties, namely Young's modulus (E) and hardness (H), were measured using nanoindentation. As shown in Figure 7e, the HT-Na_3PS_4 has an unexpected decrease in penetration depth. This "pop-in" phenomenon is correlated with the crack formation, indicating that the HT-Na_3PS_4 is more brittle compared with $Na_3PS_{3.4}O_{0.6}$. Furthermore, $Na_3PS_{3.4}O_{0.6}$ has small numerical fluctuation for E and H, confirming its homogeneous character (Figure 7f). Moreover, introducing oxygen can increase E and H since it generates bridging oxygens in the glass network, which is related to the stronger chemical bonding of P—O than that of P—S.[110] Overall, the mechanical properties of $Na_3PS_{3.4}O_{0.6}$ glass (including the shear modulus of 8.0 ± 0.3 GPa) can ensure suppressing sodium dendrite penetration.[110]

The DC-conductivity change in $Na_3Al_2P_3O_{12}$ (Na_2O-Al_2O_3-P_2O_5) glass caused by substituting Na_2SO_4 for Al_2O_3 was measured to identify the factors influencing the ionic conductivity.[111] Raman spectroscopy results show that increasing the Na_2SO_4 content can increase the fraction of isolated SO_4^{2-} units, which are charge compensated by sodium-ion (**Figure 8**a). Magic-angle spinning (MAS)-NMR results further indicate that increasing the Na_2SO_4 content also increases the content of nonbridging oxygens. These structural variations are related to the electrochemical performances. That is, interionic Coulombic interaction and SO_4^{2-} unit addition can regulate the critical hopping length of sodium-ions and thus the ionic conductivity. The correlation between the structure relaxation dynamics and the heterogeneous structure of $NaPO_3$-AlF_3 glass has been analyzed via NMR.[112] These results confirm that adding AlF_3 to the $NaPO_3$ network can increase the connectivity via increasing the number of heteronuclear Al—O—P bonds (Figure 8b). Moreover, the structural heterogeneity affects macroscopical parameters such as T_g and mechanical properties. In glasses, sodium ions have the dual role of both charge compensator and network modifier. Based on both experimental and simulation analyses, it is confirmed that the ion conductivity depends on both sodium ion concentration and charge-compensated oxygen content for the $Na_3Al_2P_3O_{12}$ glass (Figure 8c). Increasing the fraction of bridging oxygens can enhance the ionic conductivity from 3.7×10^{-8} to 3.3×10^{-7} S cm^{-1} at 100 °C.[113] Other tested glassy electrolytes for SIBs are Na_2S-P_2S_5,[114] Na_3BS_3,[115] Na_2O-P_2O_5-Al_2O_3-NaF-Na_2SO_4,[116] $Na_3Al_2P_3O_{12}$-NaF,[117] sodium borophosphate,[118] sodium borosilicate,[119] NaCl-Ga_2S_3-GeS_2,[120] Na_3PS_4-Na_4GeS_4,[121] Na_2O-B_2O_3-SiO_2-H_2O,[122] etc. Further development of glass electrolytes with both high ionic conductivity and good machinability is required in the future. Generally, achieving this goal is challenging for a single material. The most effective strategy will likely be to develop multicomponent composite glass electrolytes. It may also be a promising route to combine these with traditional polymer electrolytes.

Finally, we note that glasses can also be used as the cathode materials for SIBs. For example, $30Na_2O$-$40FeO$-$30P_2O_5$ glass cathode displays a high discharge capacity of 115 mAh g^{-1} (Figure 8d). A higher capacity could be achieved by increasing the content of FeO in the glass.[123] Similarly, a tin-substituted vanadate glass as cathode material also shows sodium ion storage activity.[124] Given the limited number of developed cathodes,

© 2023 The Authors. Small published by Wiley-VCH GmbH

16136829, 0, Downloaded from https://onlinelibrary.wiley.com/doi/10.1002/smll.202304270 by Aalborg University Library, Wiley Online Library on [06/12/2023]. See the Terms and Conditions (https://onlinelibrary.wiley.com/terms-and-conditions) on Wiley Online Library for rules of use; OA articles are governed by the applicable Creative Commons License

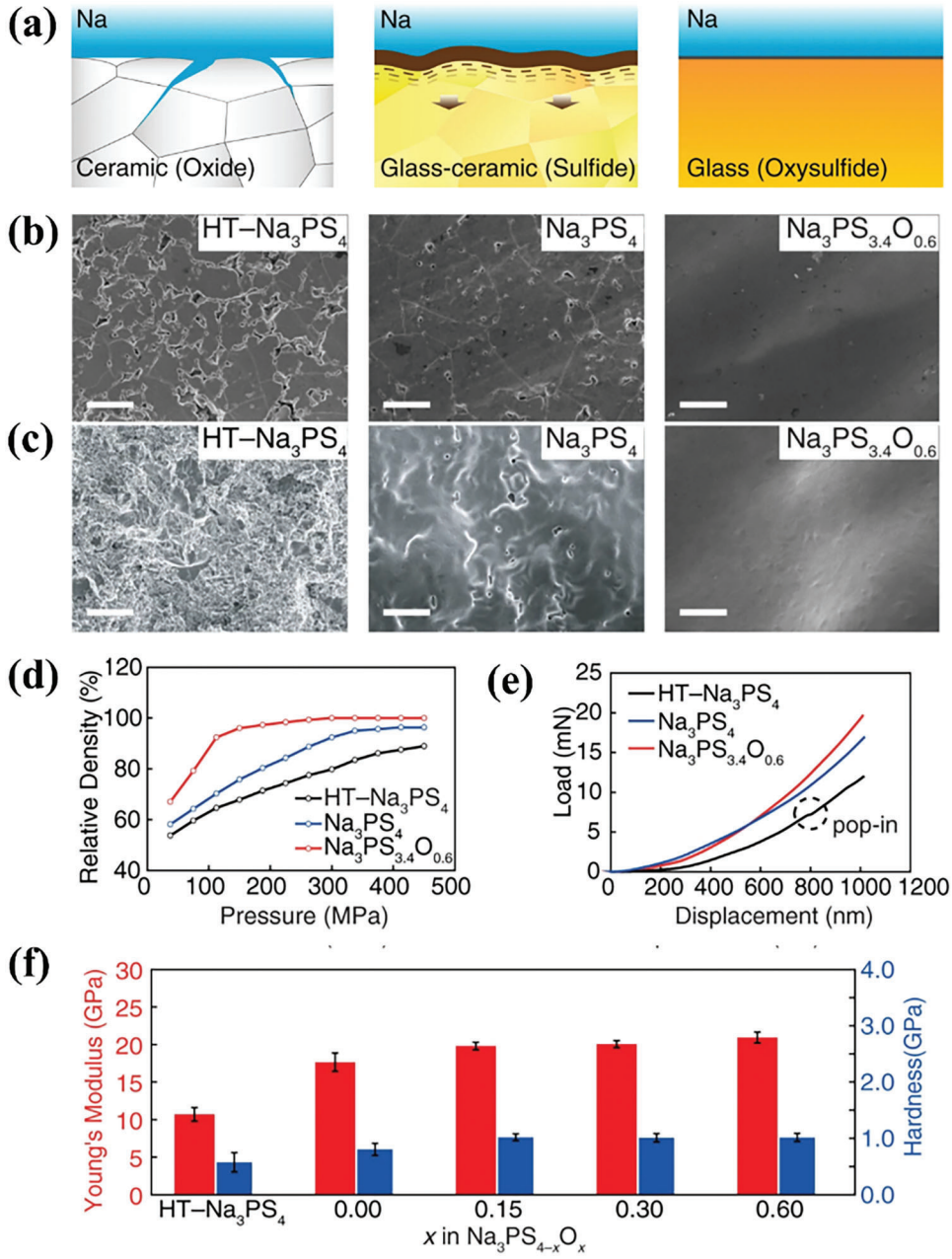

Figure 7. a) Three types of solid electrolyte-sodium metal interfaces. b) Surface morphology of different solid electrolytes. c) Cross-section morphology of different solid electrolytes. d) Density versus preparation pressure. e) Nanoindentation loading versus displacement. f) Young's modulus and hardness variation with composition. (a–f) were reproduced with permission.[110] Copyright 2022, Springer Nature.

this is a research direction with numerous unexplored possibilities. Fortunately, we can take inspiration from the glass cathode materials that have been developed for LIBs.

3.5.2. Non-glass AMs for Sodium Batteries

Non-glassy AMs are also widely used as anode and cathode material in sodium batteries. Particularly, amorphous carbon materials are extensively studied.[127] The structure of amorphous carbons can affect the sodium storage performance and mechanism.[128] In addition, amorphous $Sn_{0.5}Ge_{0.5}P_3$ with durable cycle stability has been studied. This material shows the ordered cation arrangement and anion distribution on the short-range length scale, while the long-range disorder facilitates the ion diffusion (Figure 8e).[125] Therefore, amorphous $Sn_{0.5}Ge_{0.5}P_3$ has a high capacity of 1132 mAh g^{-1} at 0.1 A g^{-1}. Even at 10 A g^{-1}, its capacity still reaches 321 mAh g^{-1}. According to the simulation results, the amorphous Fe_2O_3 has a much lower intercalation energy of 1.82 eV compared with crystal Fe_2O_3

© 2023 The Authors. Small published by Wiley-VCH GmbH

16136829, 0, Downloaded from https://onlinelibrary.wiley.com/doi/10.1002/smll.202304270 by Aalborg University Library, Wiley Online Library on [06/12/2023]. See the Terms and Conditions (https://onlinelibrary.wiley.com/terms-and-conditions) on Wiley Online Library for rules of use; OA articles are governed by the applicable Creative Commons License

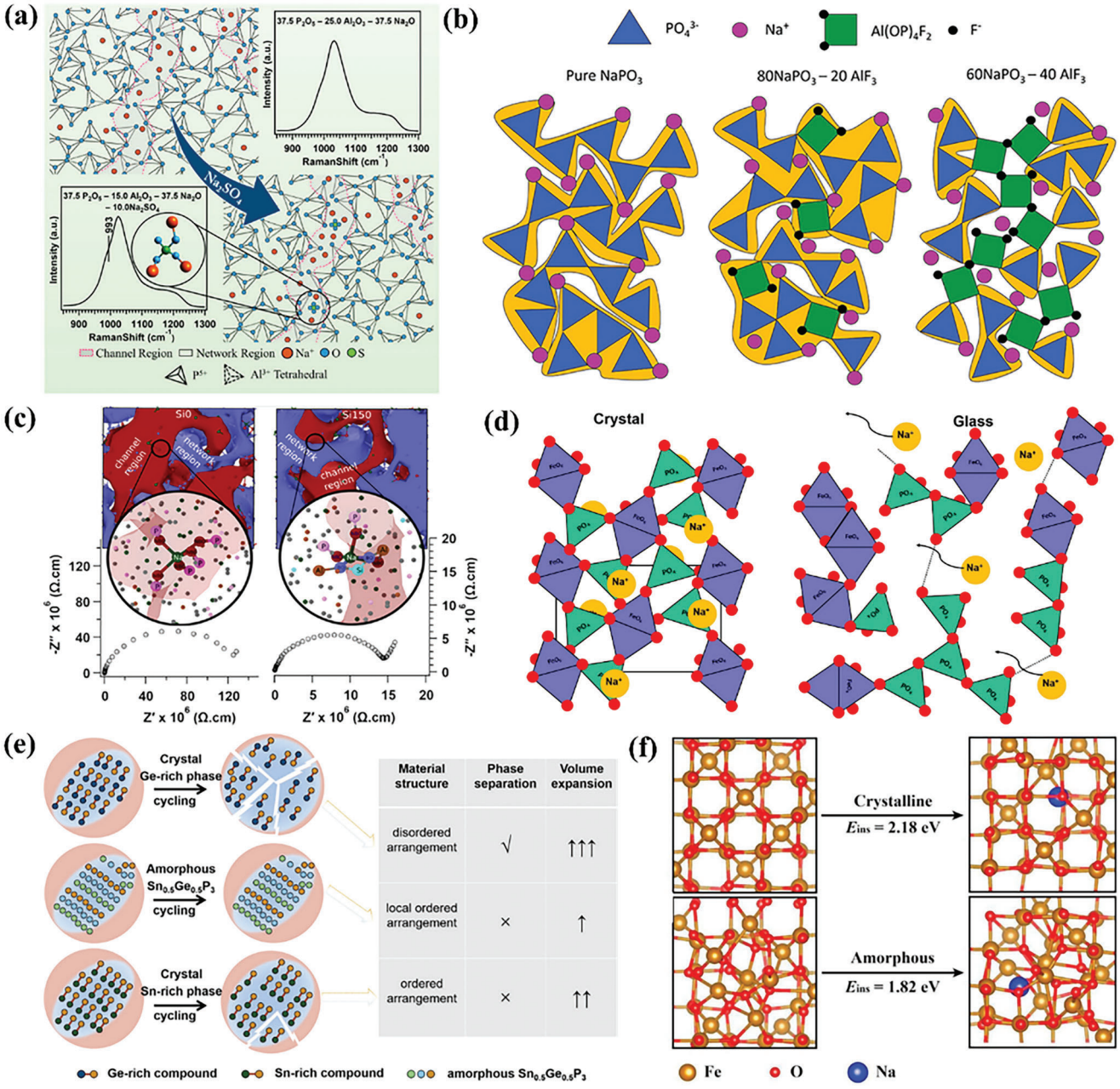

Figure 8. (a) Structure and Raman spectra of Na_2SO_4 on $Na_3Al_2P_3O_{12}$ glasses. Reproduced with permission.[111] Copyright 2022, Frontiers Media S.A. b) Structure of pure $NaPO_3$, $80NaPO_3$–$20AlF_3$, and $60NaPO_3$–$40AlF_3$ glasses. Reproduced with permission.[112] Copyright 2019, Frontiers Media S.A. c) Atomic structure of glassy $Na_3Al_2P_3O_{12}$ samples and the corresponding impedance spectra. Reproduced with permission.[113] Copyright 2021, American Chemical Society. d) Sodium ion conduction in glassy and crystal sodium iron phosphate. Reproduced with permission.[123] Copyright 2016, Elsevier. e) Structure evolution for two crystalline phases and the amorphous $Sn_{0.5}Ge_{0.5}P_3$. Reproduced with permission.[125] Copyright 2021, American Chemical Society. f) Geometry structure change of crystalline and amorphous Fe_2O_3 during the sodium-ion intercalation. Reproduced with permission.[126] Copyright 2019, Elsevier.

(2.81 eV), indicating that the sodium ion intercalation is easier in the case of amorphous Fe_2O_3 (Figure 8f). As a proof of the simulation prediction, a porous amorphous Fe_2O_3 based composite anode was fabricated.[126] The obtained composite anode delivers a high capacity of 408 mAh g^{-1} at 100 mA g^{-1} and good rate performance, which is consistent with the results of amorphous Fe_2O_3/graphene composite nanosheets.[129]

It is well known that the intrinsic strain of a material is closely connected with the degree of order and crystal type (single crystal and polycrystal), which also affects the structural stability (**Figure 9**a). For the 2D amorphous GeS_2, the amorphous matrix can enhance the uniform distribution of intermediate interface and alleviate active material aggregation. Furthermore, amorphous GeS_2 has sufficient isotropic sodium ion transfer

© 2023 The Authors. Small published by Wiley-VCH GmbH

16136829, 0, Downloaded from https://onlinelibrary.wiley.com/doi/10.1002/smll.202304270 by Aalborg University Library, Wiley Online Library on [06/12/2023]. See the Terms and Conditions (https://onlinelibrary.wiley.com/terms-and-conditions) on Wiley Online Library for rules of use; OA articles are governed by the applicable Creative Commons License

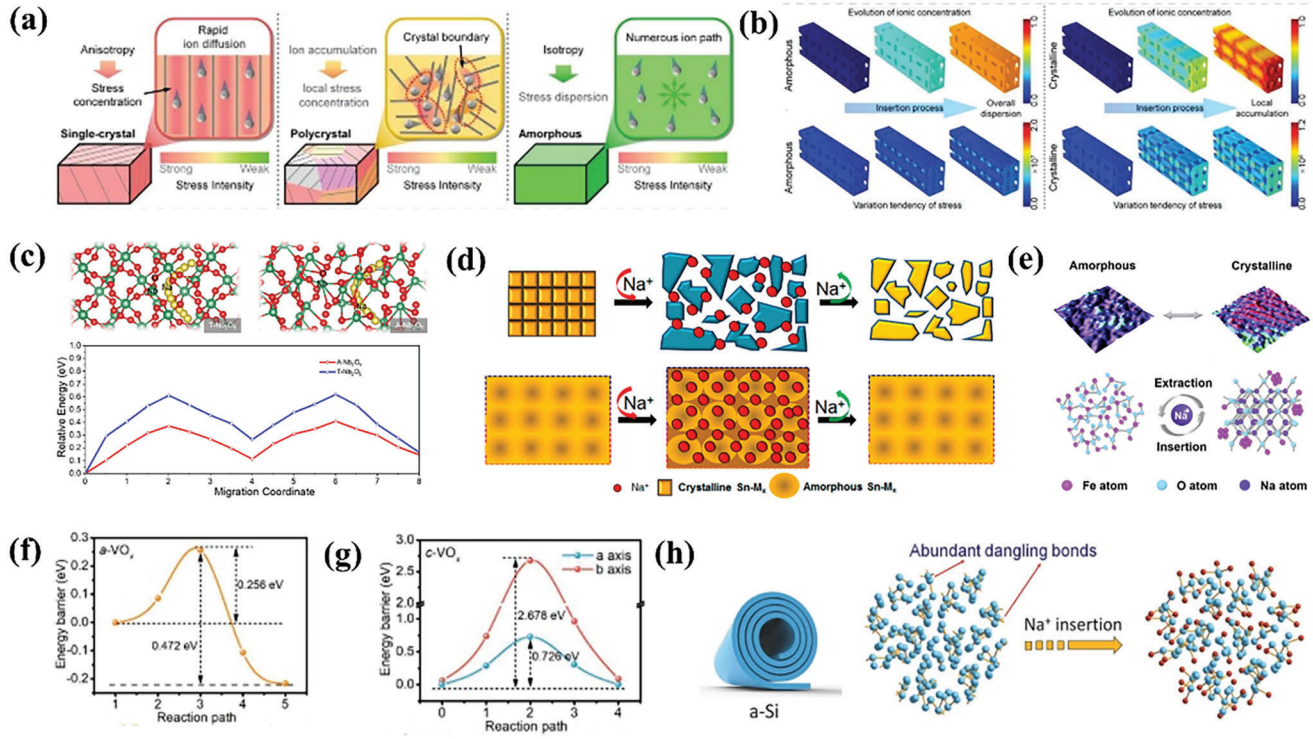

Figure 9. a) Stress distribution and ion transfer of single crystal, polycrystal, and amorphous structures during intercalation/extraction processes. b) Simulation results of ion concentration and stress distribution for amorphous and crystal structures. (a) and (b) were reproduced with permission.[130] Copyright 2022, Wiley-VCH GmbH. c) Sodium-ion migration configuration and the related energy barrier for amorphous and orthogonal Nb_2O_5. Reproduced with permission.[131] Copyright 2021, Elsevier. d) Obvious pulverization challenge for crystalline alloys/metals and the improved stability of amorphous nanoalloy. Reproduced with permission.[132] Copyright 2015, American Chemical Society. e) Amorphous FeO_x nanosheets featuring the reversible structure transformation during sodium-ion storage. Reproduced with permission.[133] Copyright 2020, Elsevier. f,g) Sodium-ion migration energy barrier for amorphous and crystal VO_x, respectively. (f) and (g) were reproduced with permission.[134] Copyright 2021, Wiley-VCH GmbH. h) Schematic of sodium storage for amorphous Si. Reproduced with permission.[135] Copyright 2018, Wiley-VCH GmbH.

channels and storage sites and can accommodate the volume change, thereby inhibiting the stress generation. To verify the role of the structural disorder in ion diffusion and stress generation in battery during cycling, the comparison between amorphous and crystalline GeS_2 was made by simulation using COMSOL.[130] For amorphous GeS_2, the model color is changed from blue to orange/red, and the corresponding ion concentration gradually increases. The color is uniformly distributed, demonstrating that sodium ions undergo uniform diffusion at all-direction. Similarly, the amorphous structure can cause homogeneous stress dispersion after sodium storage (Figure 9b). Hence, the local stress of crystal structure is much higher than that of amorphous structure. As expected, amorphous GeS_2 exhibits the high-rate performance and long cycling stability. Therefore, amorphization is a promising approach to construct robust and fast diffusion channels in electrode materials.

Similarly, amorphous Nb_2O_5 features the fast sodium storage with the lower ion migration energy barrier compared with crystalline Nb_2O_5 (Figure 9c).[131] Even for metal alloy anode, amorphous Co_3Sn_2 nanoalloys have better sodium storage performance than the crystalline counterparts.[132] The enhanced performance of amorphous nanoalloys is related to the facile ion accessibility and good strain accommodation (Figure 9d). Interestingly, different from amorphous FeO_x/carbon nanofiber,[136] FeO_x nanosheets[133] can undergo reversible amorphous-crystalline structure changes during sodium ion storage and hence have a high capacity of 263.4 mAh g^{-1} and long cycling stability (Figure 9e). In most cases, AMs, e.g., amorphous VO_x and Si, can maintain their disordered structure unchanged during the process of storing sodium ions. Amorphous VO_x can enable reversible and fast sodium ion intercalation/deintercalation owing to sufficient vacancy, open channel, and low diffusion barrier (Figure 9f,g).[134] For the rolled-up amorphous Si, it is subjected to a very small volumetric change during sodium storage (Figure 9h).[135] Amorphous hollow silicon nanospheres produced via low-temperature synthesis can also enhance the cycling stability of batteries.[137] There are many other reported amorphous anode materials such as MoS_x,[138] P_2S_5,[139] MoS_3,[140] MoS_2-MoO_3-carbon,[141] FeOOH,[142] $CuSnO_3$,[143] CoS,[144] $CoMoS_4$,[145] Co_2P,[146] Bi_2S_3,[147] P_4SSe_2,[148] antimony (Sb),[149] Sb_2S_3,[150] Sb_2Se_3,[151] SnSe,[152] $Sn_2P_2O_7$,[153] SnO_2,[154] TiO_2,[155] V_2O_5,[156] VO_2,[157] $Zn_2V_2O_7$,[158] phosphorus (P),[159] Co—Sn—S,[160] SnO_xP_y,[161] SnO_x,[162] zinc oxysulfide,[163] etc. In the future, it is necessary to further evaluate the index parameters of the reported amorphous anode materials from the perspective of commercialization.

As a promising cathode candidate of SIBs, amorphous $FePO_4$ has been reported by several research groups.[164] Constructing

© 2023 The Authors. Small published by Wiley-VCH GmbH

16136829, 0, Downloaded from https://onlinelibrary.wiley.com/doi/10.1002/smll.202304270 by Aalborg University Library, Wiley Online Library on [06/12/2023]. See the Terms and Conditions (https://onlinelibrary.wiley.com/terms-and-conditions) on Wiley Online Library for rules of use; OA articles are governed by the applicable Creative Commons License

mesoporous structure[165] and introducing lattice water[166] can further enhance the performance of $FePO_4$. Recently, a fascinating case was demonstrated,[167] where the thermodynamical stable but electrochemically inactive Maricite ($NaFePO_4$) was transformed into the electrochemically active state via an amorphization process realized by high-energy ball-milling. The amorphization process greatly enhances sodium storage and transfer kinetics in the Maricite-based cathode, leading to the sodium storage capacity of 115 mAh g^{-1} at 1C and excellent cycling stability manifested by the capacity retention of 91.3% after 800 cycles. By the X-ray absorption near edge spectroscopy (XANES) and Raman, the origin of the enhancement of the electrochemical performances has been discovered,[167] i.e., the transformation of edge-sharing FeO_6 octahedra into various FeO_n polyhedra. This discovery is crucial for developing superior energy storage materials through disorder engineering. Amorphous $FeVO_4$,[168] $NaVOPO_4$,[169] NaF-$FeSO_4$,[170] Na_2TiS_3,[171] MnO_2,[172] and iron phosphate[173] materials are also proposed as the cathodes of SIBs. Notably, sulfur in amorphous silica[174] and amorphous selenium restrained by biomass-carbon[175] were reported to construct room-temperature Na—S and stable Na–Se batteries, respectively. Given that the research on AMs for sodium battery cathodes is still in its infancy, combining theoretical calculations and experimental analysis can increase the speed of developing high-performance amorphous storage sodium cathodes. For example, it would be valuable to analyze the sodium diffusion and storage characteristics in the well-studied layered oxide cathodes, Prussian blue analogues, and polyanion cathodes, when these can be obtained in an amorphous state. Such screening could be done using high-throughput simulations and then the most promising amorphous cathode materials could be synthesized with the tailored structures.

3.5.3. AMs for Potassium Batteries

Amorphous carbon materials again have merits of low cost and high potassium-ion insertion/extraction reversibility.[176] Via disorder engineering, the amorphous carbon/graphite coupled framework has been successfully used to enhance electrochemical properties of the potassium batteries.[177] Amorphous carbon can store potassium ions and accommodate the volume expansion/shrinkage, thereby enhancing its capacity and cycling stability. The strain optimization process in the amorphous carbon/graphite anode was found to occur by analyzing distribution stress contours after potassium ion intercalation via the finite element simulation (**Figure 10**a). Taking advantages of large interlayer distance, sufficient active site, and easily accessible surface, the amorphous carbon/graphite coupled framework delivers the high capacity of 358.4 mAh g^{-1}, excellent rate performance (272.2 mAh g^{-1} at 1 A g^{-1}), and high cycle stability (1800 cycles). Similarly, amorphous MoS_3 with 1D chain displays different reaction processes for potassium storage compared with the crystal 2H-MoS_2 (Figure 10b).[178] To understand the internal mechanism of amorphous MoS_3 with the improved rate performance, reversible capacity, and cycle stability, the potassium adsorption and diffusion on the 1D MoS_3 has been simulated. According to the simulated adsorption energy values, the potassium ion adsorption on the 1D MoS_3 is stronger than that of MoS_2 (Figure 10c,d). Meanwhile, potassium ions easily diffuse along 1D MoS_3 chains (Figure 10e). The potassium migration energy barrier on the 1D MoS_3 is 0.043 eV, being significantly lower than that of 2H-MoS_2 (0.088 eV). The low diffusion energy barrier facilitates potassium ion transport and thus enhances rate performances. The anodes made from amorphous cobalt (Co),[179] $CoS_{1.4}$,[180] $FeVO_4$,[181] tellurium (Te),[182] VS_4,[183] and SnS[184] have also been fabricated to store potassium ions. Overall, the research of AMs for potassium batteries is in its infancy. In view of the similar working principles of potassium batteries and lithium/sodium batteries, it is expected that an increasing number of amorphous anodes, electrolytes, and cathodes will be used in potassium batteries in the future.

3.6. AMs for Zinc Batteries

Due to the moderate redox potential of zinc, zinc-based batteries can directly use aqueous electrolytes, thus possessing intrinsically higher safety. Considering that the ionic conductivity of aqueous electrolytes is much higher than that of organic electrolytes and solid electrolytes, aqueous zinc-based batteries have higher power densities. Intrinsically high safety and high-power density make zinc-based batteries promising for large-scale energy storage and flexible electronics. However, the metallic zinc anodes of aqueous zinc batteries suffer from dendrite growth and chemical/electrochemical corrosion. To this end, Bi_2O_3-Li_2O-ZnO and Bi_2O_3-ZnO-CaO glasses have both been synthesized to serve as the functional coating layers of zinc particle anodes for alkaline zinc batteries.[185] Due to the high theoretical specific energy of zinc–air battery (about 1086 Wh kg^{-1}), a silver-copper metallic glass based electrocatalyst was developed to obtain the high-performance zinc–air battery with high activity and stability.[186] In addition, an amorphous silicon nitride (SiN_x) with silicon dangling bond was fabricated to enhance the zinc anode stability in a mildly acidic electrolyte.[187] The Si dangling bonds and zincophilic nitrogen sites can evenly distribute the zinc ions and enable uniform zinc plating. Meanwhile, the electrochemical inertness of SiN_x can also inhibit unwanted side reactions (**Figure 11**a). DFT results reveal that the zinc adsorption energies on the silicon dangling bond (−2.26 eV) and nitrogen site (−2.17 eV) of SiN_x are much lower than those of Zn (101) and Si (010), thus allowing suppressing the zinc atom aggregation (Figure 11b). The electrical field and zinc-ion distribution is further analyzed via COMSOL Multiphysics. The electrical field and zinc ion distributions of the SiN_x@Zn are more homogeneous compared with those of the pure zinc, achieving uniform zinc plating and thus increase cycle stability of SiN_x@Zn (Figure 11c,d). The above-mentioned work confirms the importance of using an artificial protective layer with defect sites in suppressing zinc dendrites. The effectiveness of the commercial amorphous silicon nitride layer was confirmed.[188] Similarly, amorphous aluminum nitride and ZnO have also been proposed to inhibit the dendrite growth and corrosion.[189]

Given that zinc anode can be processed and treated in an ambient environment, it provides a broad application space for amorphous materials, especially glass materials. Therefore, studies should be conducted by involving in situ construction of the amorphous layer, which has the strong adhesion to zinc anode

© 2023 The Authors. Small published by Wiley-VCH GmbH

16136829, 0, Downloaded from https://onlinelibrary.wiley.com/doi/10.1002/smll.202304270 by Aalborg University Library, Wiley Online Library on [06/12/2023]. See the Terms and Conditions (https://onlinelibrary.wiley.com/terms-and-conditions) on Wiley Online Library for rules of use; OA articles are governed by the applicable Creative Commons License

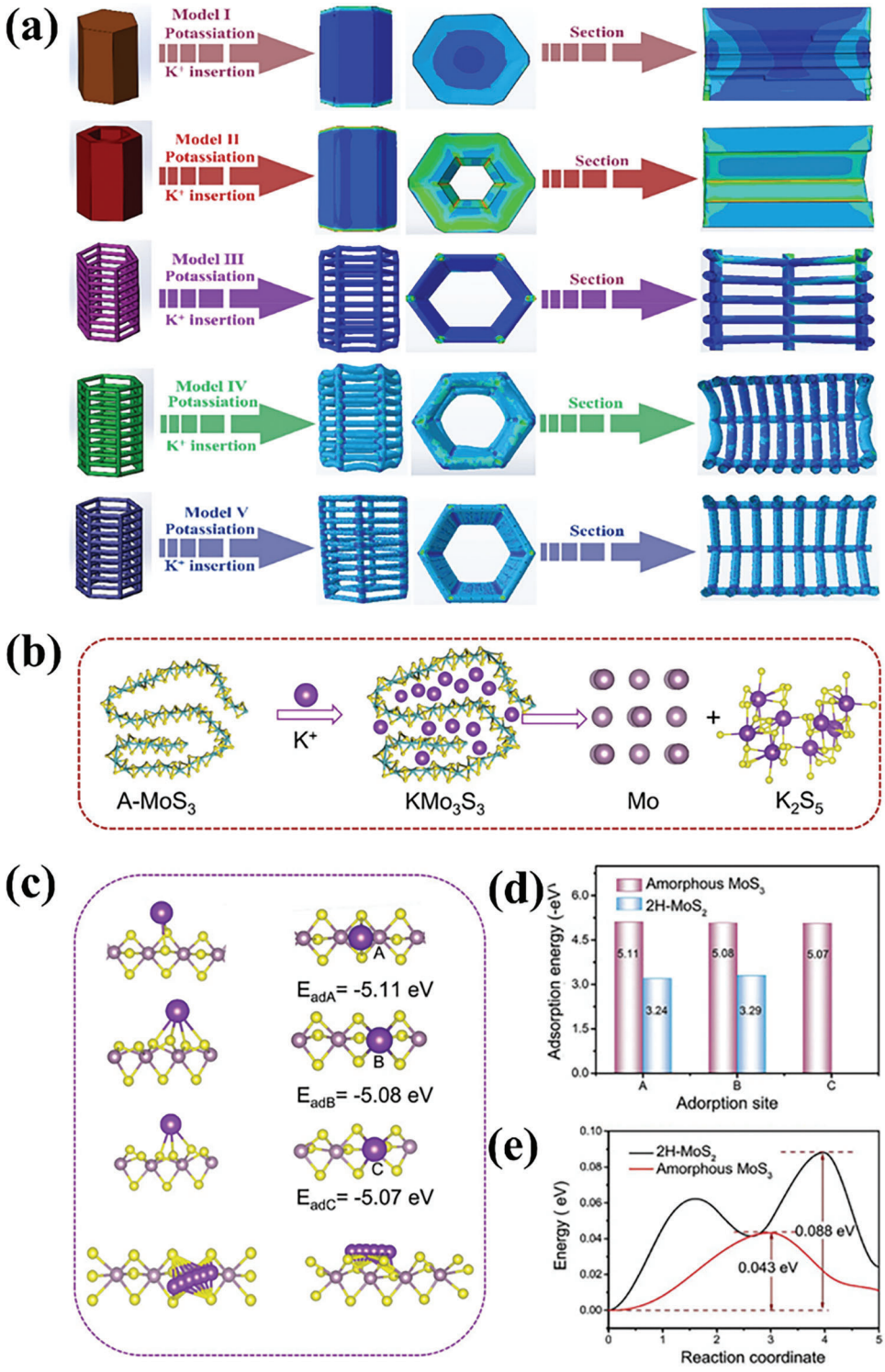

Figure 10. a) Overall and cross section stress contours of five models as determined from finite element simulations. Reproduced with permission.[177] Copyright 2021, Elsevier. b) Conversion mechanism of amorphous MoS_3. c) Potassium adsorption and migration energy for amorphous MoS_3. d,e) Comparison of potassium adsorption energy and migration energy, respectively. (b–e) were reproduced with permission.[178] Copyright 2022, Wiley-VCH GmbH.

© 2023 The Authors. Small published by Wiley-VCH GmbH

16136829, 0, Downloaded from https://onlinelibrary.wiley.com/doi/10.1002/smll.202304270 by Aalborg University Library, Wiley Online Library on [06/12/2023]. See the Terms and Conditions (https://onlinelibrary.wiley.com/terms-and-conditions) on Wiley Online Library for rules of use; OA articles are governed by the applicable Creative Commons License

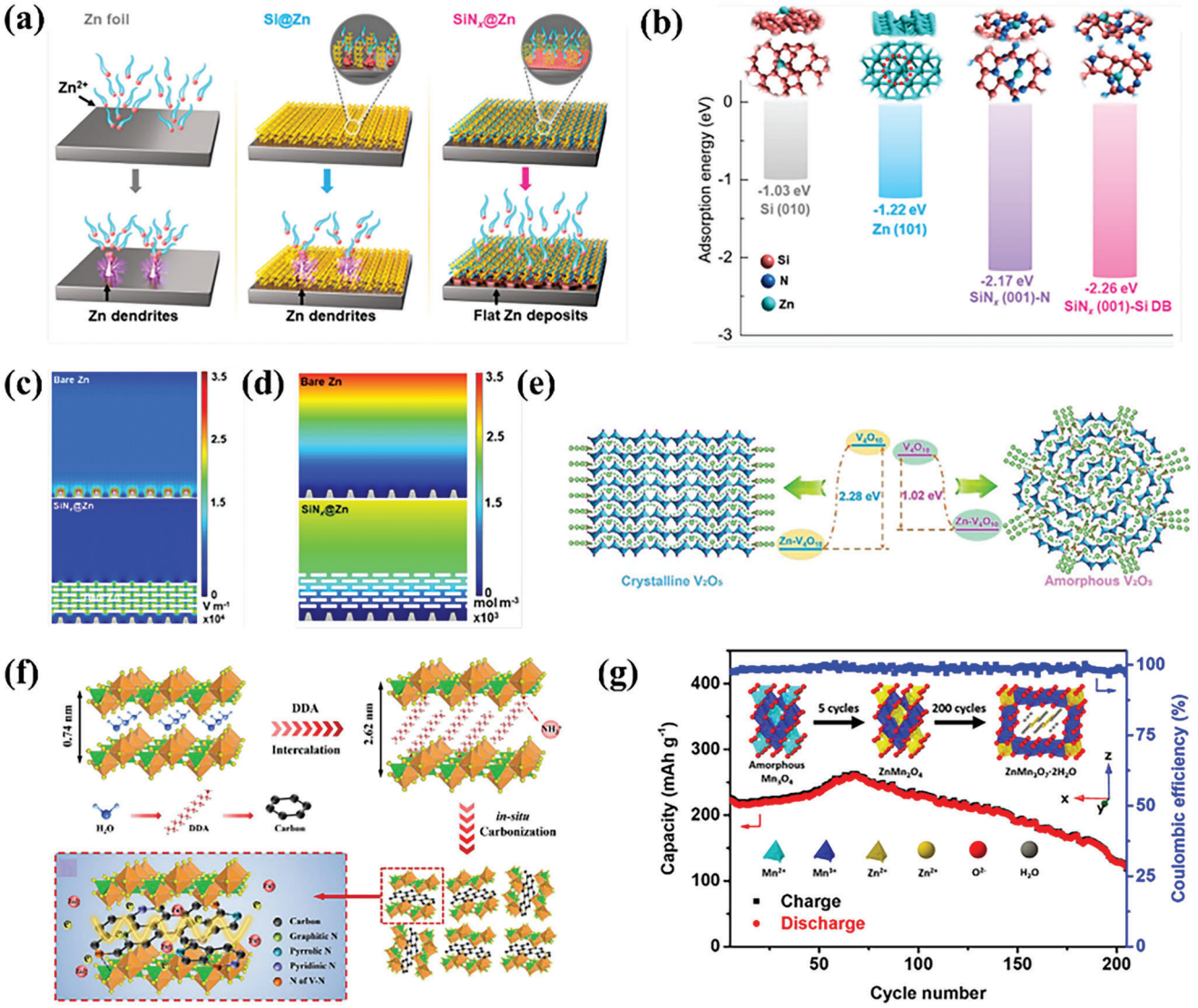

Figure 11. a,b) Schematics of zinc plating and adsorption energy of zinc atoms on pure Zn, Si@Zn, and SiNx@Zn, respectively. c,d) Surface electrical and zinc-ion ion fields of pure Zn and SiN_x@Zn, respectively. (a–d) were reproduced with permission.[187] Copyright 2022, American Chemical Society. e) Zinc-ion diffusion and intercalation/deintercalation energy for crystal and amorphous V_2O_5 cathodes. Reproduced with permission.[190] Copyright 2020, Wiley-VCH GmbH. f) Preparation of amorphous vanadyl phosphate/carbon superlattice cathode with fast pseudocapacitive zinc-ion storage. Reproduced with permission.[191] Copyright 2021, Elsevier. g) Cycling performance and storage zinc mechanism of amorphous Mn_3O_4 cathode. Reproduced with permission.[192] Copyright 2020, American Chemical Society.

surface. For example, the effective amorphous interface layer can be constructed on the zinc anode surface by using conventional post-treatment and processing methods of AMs.

As a cathode material of aqueous zinc-ion batteries, amorphous V_2O_5 with isotropic zinc-ion diffusion pathways and active sites exhibits fast zinc-ion transport and high capacity.[193] First principles calculations reveal that crystalline V_2O_5 delivers a higher zinc insertion energy barrier compared with amorphous V_2O_5 (Figure 11e).[190] In addition, the introduction of phosphorus element can further activate the amorphous V_2O_5 cathode.[194] Impressively, by constructing amorphous V_2O_5-graphene heterostructures, both the storage zinc capacity and rate performance can be simultaneously increased.[195] Furthermore, an amorphous superlattice of vanadyl phosphate ($VOPO_4$)/carbon having dominant pseudo-capacitance zinc storage has been reported (Figure 11f).[191] Besides vanadium-based cathodes, the mesoporous amorphous manganese oxide (Mn_3O_4) cathode also exhibits a capacity of 222 mAh g^{-1}, good cyclability, and high discharge platform. Electrochemical and structural analyses confirm that the sequent conversion reactions occur after different cycles (Figure 11g).[192] Additionally, it has been demonstrated that amorphous MnO_2 can be used as an advanced cathode material for aqueous zinc-ion batteries.[196] Amorphous Ni—Co—S,[197] V_xO_y,[198] hydrated vanadium oxide,[199] and Fe—V—O[200] cathodes have also been reported. Furthermore, amorphous carbon,[201] cobalt nitride,[202]

© 2023 The Authors. Small published by Wiley-VCH GmbH

16136829, 0, Downloaded from https://onlinelibrary.wiley.com/doi/10.1002/smll.202304270 by Aalborg University Library, Wiley Online Library on [06/12/2023]. See the Terms and Conditions (https://onlinelibrary.wiley.com/terms-and-conditions) on Wiley Online Library for rules of use; OA articles are governed by the applicable Creative Commons License

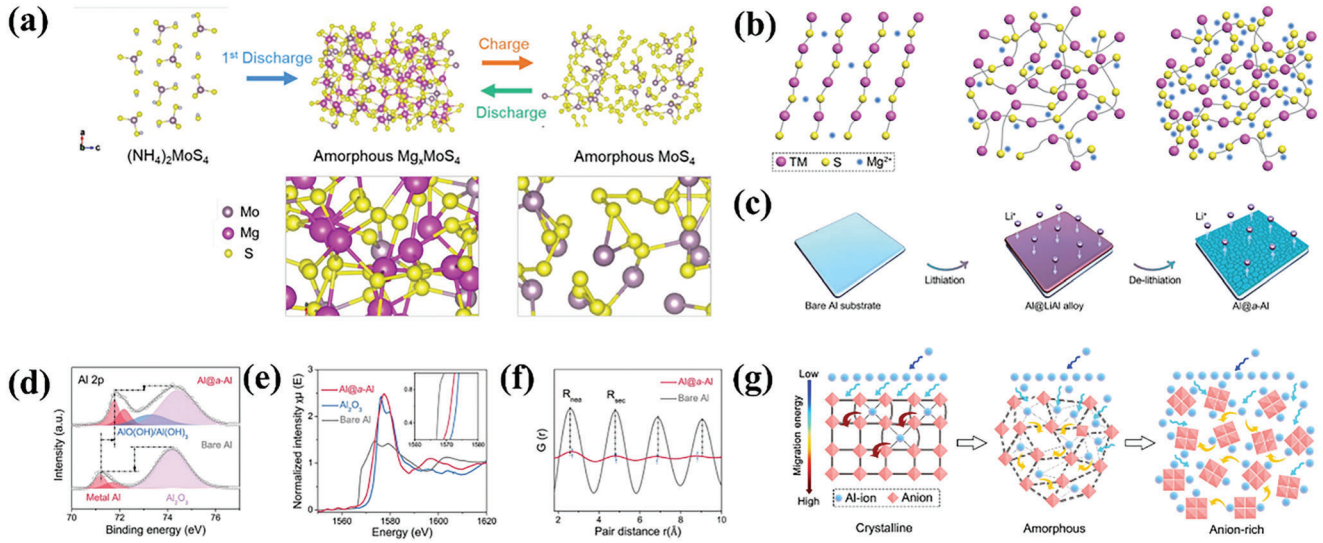

Figure 12. a) Reversible magnesium-ion storage mechanism between amorphous MoS_4 and $Mg_{1.6}MoS_4$. Reproduced with permission.[211] Copyright 2022, American Chemical Society. b) Magnesium-ion intercalation into crystal transition metal sulfides, amorphous transition metal sulfides, and amorphous transition metal polysulfides. Reproduced with permission.[212] Copyright 2021, American Chemical Society. c) Fabrication of the Al@amorphous aluminum anode. d–f) Al 2p X-ray photoelectron spectroscopy (XPS) spectra, Al K-edge X-ray absorption near-edge structure (XANES) spectra, and the radial distribution function (RDF) profiles of Al@amorphous aluminum and pure Al, respectively. (c–f) were reproduced with permission.[29] Copyright 2022, American Chemical Society. g) Aluminum-ion storage and migration in crystalline, amorphous, and amorphous anion-rich materials. Reproduced with permission.[218] Copyright 2021, American Association for the Advancement of Science (AAAS).

$CoSe_2$,[203] cobalt phosphate,[204] CoFe-phosphate,[205] Fe(III)-borate,[206] and Ni—Co—Fe hydroxide[207] have been fabricated and tested for zinc–air batteries. The quantitative comparison of zinc battery performances is shown in Table S6 in the Supporting Information. Considering the use of aqueous electrolytes for Zn-based batteries, it is necessary to develop AMs with excellent stability in different pH environments to improve the cycle stability. While this has not been explored in detail in the case of amorphous battery materials, there is a rich literature on understanding the chemical durability of AMs, for example in the field of nuclear waste immobilization.[208] Studies have shown that the aqueous stability is related to the number of topological constraints per atom in the network.[209] This physical understanding knowledge can be leveraged and used as input for physics-informed machine learning algorithms[210] to predict the dissolution rate of Zn-based battery materials.

3.7. AMs for Other Types of Batteries

There are also other types of multivalent ion batteries such as magnesium-, calcium-, and aluminum-based batteries. They all have their own characteristics and play a role in specific application fields. For example, magnesium batteries with low cost are promising for large-scale energy-storage. An amorphous ammonium tetrathiomolybdate ($(NH_4)_2MoS_4$) with abundant active sites and open transport paths has been reported.[211] The covalent-like Mo—S bonds can weaken the magnesium cation interaction and accelerate the kinetics. They also can promote the molybdenum- and sulfur-participating redox reactions at the same time, resulting in a high capacity. The obtained $(NH_4)_2MoS_4$ delivers high capacity (333 mAh g^{-1}) and good rate performance (≈15 C). **Figure 12**a shows its working mechanism, i.e., amorphous MoS_4 is created during the initial discharging process along with the NH_4^+ extraction, and then the subsequent redox reaction occurs between amorphous MoS_4 and Mg_xMoS_4. Interestingly, the strategy of both amorphization and anion enrichment has been reported to strengthen the bulk ion diffusion, provide more active sites, and increase the local electron transfer via the extra anionic redox center (Figure 12b). As a proof of concept, different amorphous titanium polysulfide (a-TiS_x) materials have been prepared, showing enhanced performances in comparison to their crystalline counterparts. The ion storing mechanism is the combined conversion/intercalation reaction with the coexisting cationic (Ti) and anionic (S) redox chemistry.[212] Furthermore, amorphous V_2O_5,[213] V_2O_5-P_2O_5,[214] and CoS_x[215] are reported to store magnesium. It has also been shown that amorphous titanium dioxide and silicon are more favorable for magnesium storage compared with their crystalline counterparts.[216] Impressively, both MgS-P_2S_5-MgI_2 glass and amorphous magnesium borohydride are good magnesium ion conductors.[217]

Aluminum batteries are one of the most sustainable electrochemical storage systems. An amorphization strategy has been reported to obtain high-performance metallic aluminum anode. Based on the operando lithium alloying/dealloying reaction, the artificial amorphous aluminum (a-Al) layer could be obtained (Figure 12c).[29] The peaks of Al^0 shift to higher binding energy position for aluminum with amorphous layer (Al@a-Al) compared with those of the pure Al metal, confirming the atomic disorder of the artificial amorphous layer phase (Figure 12d). XANES analysis further demonstrates that Al@a-Al has a higher energy value than that of pure Al, indicating poor periodicity (Figure 12e). Analysis of the radial distribution function (RDF) shows that the nearest and the second nearest neighboring peaks

© 2023 The Authors. Small published by Wiley-VCH GmbH

16136829, 0, Downloaded from https://onlinelibrary.wiley.com/doi/10.1002/smll.202304270 by Aalborg University Library, Wiley Online Library on [06/12/2023]. See the Terms and Conditions (https://onlinelibrary.wiley.com/terms-and-conditions) on Wiley Online Library for rules of use; OA articles are governed by the applicable Creative Commons License

Table 1. The mechanical, electrochemical, chemical, and thermal properties of some typical AMs for batteries.

Materials[a)]	Mechanical properties	Electrochemical properties	Chemical properties	Thermal properties
ZIF-62 glass (Co)	–	306 mAh g^{-1} at 2 A g^{-1} 1000 cycles Anode of LIBs[26a]	Lithium storage structure evolution	T_g = 563 K[223]
ZIF-62 glass (Zn)	E = 5.2, ν = 0.343 K_{Ic} = 0.104 γ = 0.82[224]	–	–	T_g = 593 K[225] κ = 0.130[33]
ZIF-4 glass (Zn)	–	Li^+ conductivity is 0.161 mS cm^{-1} (303 K), ZIF-4 based electrolyte[26b]	Lithium transfer stability	T_g = 570 K[225] κ = 0.115[33]
Li_2S- B_2S_3-LiI-SiO_2 glass	–	Li^+ conductivity is 2.1 mS cm^{-1} (RT)[53]	Lithium transfer stability	–
Li_2S-P_2S_5 glass	E = 18.5, H = 1.9 K_{Ic} = 0.23[52]	Li^+ conductivity at 10^{-1} mS cm^{-1} level[226]	Lithium transfer stability	–
Amorphous polymer	–	Li^+ conductivity is about 0.36 mS cm^{-1} (RT)[25]	Lithium transfer stability	Thermal stability (652 K)
P_2O_5-Al_2O_3-Na_2O glass	–	Na^+ conductivity is 1.39 ×10^{-4} mS cm^{-1} (373 K)[111]	Sodium transfer stability	–
$Na_3PS_{3.4}O_{0.6}$ glass	E = 20.9, H = 1.0 ν = ≈0.3, G = 8.0	Na^+ conductivity is 8.2 ×10^{-2} mS cm^{-1} (333 K)[110]	Sodium transfer stability	–
Amorphous GeS_2	–	513 mAh g^{-1} at 10 A g^{-1} 1000 cycles Anode of SIBs[130]	Sodium storage stability	–

[a)] Elastic modulus (E, GPa), hardness (H, GPa), Poisson's ratio (ν), shear modulus (G, GPa), fracture toughness (K_{Ic}, MPa $m^{1/2}$), fracture surface energy (γ, J m^{-2}), thermal conductivity (κ, W m^{-1} K^{-1}), and room temperature (RT).

of Al@a-Al are broader and shifted in comparison of those for the crystalline bare Al (Figure 12f). Similar to the above-mentioned magnesium batteries, amorphous titanium polysulfides (a-TiS_x) with defects and anionic redox centers can also be used as cathode in aluminum-ion batteries (Figure 12g).[218] Moreover, amorphous red phosphorous,[219] V_2O_5,[220] and $FeCoS_x$[221] have been reported for aluminum batteries. Finally, besides metal-ion batteries, AMs can also be applied for nonmetal-ion storage. For example, amorphous manganese phosphate can enable high-capacity ammonium (NH_4^+) storage via the solid-liquid interfacial coordination chemistry.[222]

Table S7 in the Supporting Information provides a summary of the electrochemical properties for the battery materials discussed in this section. In general, there are ample opportunities for developing AMs for various types of batteries. Based on the research experience of lithium, sodium, potassium, and zinc batteries, advanced theoretical simulations can be applied first for preliminary screening, and then experimental verification can be used to develop AMs with different electrochemical activities and ion storage characteristics.

4. Summary and Perspectives

AMs offer the opportunity to improve the electrochemical, mechanical, chemical, and thermal properties of both lithium-ion and post-lithium-ion batteries. However, different AMs for battery applications have different electrochemical characteristics, i.e., some have high capacity, some have good cycle performance, and some have good ionic conductivity. That is, different types of batteries need AMs with specific properties. As such, it is difficult to evaluate the performances of different amorphous battery materials by using the same criteria. In other words, a common standard or criterium have not yet been fully established. Consequently, we cannot directly compare the properties of all the reported AMs, and we have therefore selected some representative examples for comparison as shown in **Table 1**. Indeed, many AMs feature good electrochemical performances as well as advantageous mechanical and thermal properties.

Based on the present review, it can be stated that three major issues remain to be addressed concerning the application of AMs in developing superior high-performance batteries: 1) The ionic conductivity and mechanical properties of amorphous solid electrolytes need to be further enhanced; 2) The electron conductivity of amorphous cathodes and anodes is still rather low; and 3) The interface resistance between electrolyte and electrode should be further reduced. Potential approaches are proposed in **Figure 13** to overcome these challenges.

By constructing glass-ceramic structure (i.e., partially crystallized glasses), the ionic conductivity and mechanical property of amorphous electrolytes can be significantly enhanced.[227] Furthermore, to fabricate superior electrolytes, ionic liquids with high ionic conductivity can be introduced into porous amorphous materials, and thus the advantages of amorphous porous materials and ionic liquids can be combined to give a synergistic effect. High-performance AM-based electrolytes can

© 2023 The Authors. Small published by Wiley-VCH GmbH

16136829, 0, Downloaded from https://onlinelibrary.wiley.com/doi/10.1002/smll.202304270 by Aalborg University Library, Wiley Online Library on [06/12/2023]. See the Terms and Conditions (https://onlinelibrary.wiley.com/terms-and-conditions) on Wiley Online Library for rules of use; OA articles are governed by the applicable Creative Commons License

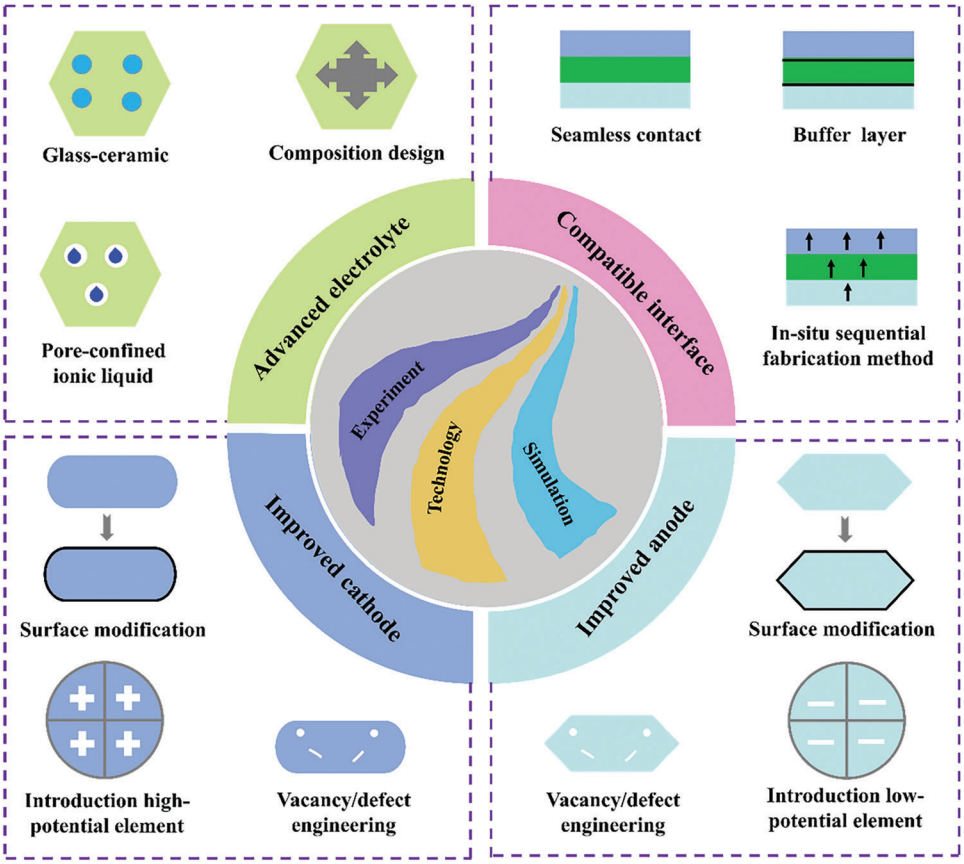

Figure 13. Promising approaches for developing advanced AM-based batteries with high performances by combing experimental, technical, and simulation (especially ML) advances.

also be obtained through component design. For example, the low-temperature paddlewheel effect in the glassy $75Li_2S$-$25P_2S_5$ electrolyte can facilitate the cation mobility.[228] Similarly, via the partial crystallization method, the performances of glassy electrode materials can be improved.[229] For example, constructing heterostructures can effectively increase the electron conductivity of AM-based electrodes.[230] To this end, MXene-AM heterostructures electrodes show enhanced performances[231] and the amorphous MXene as heterostructured electrodes present an exciting prospect.[232]

For electrode materials, applying glass-ceramic approach can achieve superior electrochemical performance.[233] Moreover, surface modification can increase the interface stability during battery cycling. By introducing defects/vacancies, the conductivity of AM-based electrodes can be improved and the number of electrochemically active sites can also be increased. Under the condition that the specific capacity remains unchanged, the energy density of the full battery can be further improved by introducing high potential elements (such as Mo[60a] and Fe[60b]) to increase the working voltage of cathode materials, and/or by applying low potential elements to reduce the working voltage of anode materials. To obtain a compatible electrolyte-electrode interface, an external force can be used to keep the electrolyte and electrode in good contact during battery working. At the same time, the interface resistance can be further reduced by constructing a buffer layer. The most ideal way would be to sequentially and in situ prepare the cathode, electrolyte, and anode layers to achieve sufficient interface contact. That is, by using the in situ synthesis step, the cathode layer (anode layer) is prepared first, then the electrolyte layer is deposited on top of it, and finally the anode layer (cathode layer) is prepared on top of the electrolyte layer.

In conclusion, AMs are some of the most promising electrolyte and electrode candidates for lithium-ion and post-lithium-ion batteries. The mechanical, electrochemical, chemical, and thermal properties can be regulated by modifying the compositions and structures of AMs. A notable advantage of AMs is that their compositions can be continuously adjusted unlike the case of stoichiometric crystals. However, efforts are still needed to further increase the battery performances, e.g., applying glass-ceramic strategies, synergistic effects, uncovering inner working mechanism, and designing high-performance amorphous electrode/electrolyte at the atomic level. Unveiling the working mechanisms of AMs for lithium-ion and post-lithium-ion batteries is one of the most urgent challenges especially for interface interactions. Fortunately, powerful analysis techniques, such as NMR, XANES, X-ray and neutron scattering, and Raman spectroscopy, are available.[29,234] Considering that AMs have the structural characteristics of short-range order, medium-range partial order, and long-range disorder, advanced simulation calculations with

© 2023 The Authors. Small published by Wiley-VCH GmbH

16136829, 0, Downloaded from https://onlinelibrary.wiley.com/doi/10.1002/smll.202304270 by Aalborg University Library, Wiley Online Library on [06/12/2023]. See the Terms and Conditions (https://onlinelibrary.wiley.com/terms-and-conditions) on Wiley Online Library for rules of use; OA articles are governed by the applicable Creative Commons License

different dimensional accuracy are needed. Combining operando experimental characterizations and theoretical simulations is a powerful way to further effectively reveal the interface reaction and interface phase. Through understanding the working principles of AMs as electrolytes/electrodes as well as providing more insights into constructing compatible electrolyte–electrode interfaces, superior AM-based batteries can be developed in the future.

Supporting Information

Supporting Information is available from the Wiley Online Library or from the author.

Acknowledgements

This work was financially supported by Marie Skłodowska-Curie Individual Fellowship (No. 101017990) and Independent Research Fund Denmark (1127–00003).

Conflict of Interest

The authors declare no conflict of interest.

Keywords

amorphous materials, battery materials, electrochemical properties, mechanical properties, structural disorder

Received: May 22, 2023
Revised: September 16, 2023
Published online:

[1] a) Y. S. Meng, V. Srinivasan, K. Xu, *Science* **2022**, *378*, eabq3750; b) L. Wang, T. Liu, T. Wu, J. Lu, *Nature* **2022**, *611*, 61; c) C. Gao, P. Wang, Z. Wang, S. K. Kær, Y. Zhang, Y. Yue, *Nano Energy* **2019**, *65*, 104032.
[2] C. Gao, Z. Jiang, P. Wang, L. R. Jensen, Y. Zhang, Y. Yue, *Nano Energy* **2020**, *74*, 104868.
[3] Y. T. Malik, S. Y. Shin, J. I. Jang, H. M. Kim, S. Cho, Y. R. Do, J. W. Jeon, *Small* **2023**, *19*, 2206141.
[4] M. Shang, O. G. Shovon, F. E. Y. Wong, J. Niu, *Adv. Mater.* **2023**, *35*, 2210111.
[5] R. Chen, Q. Li, X. Yu, L. Chen, H. Li, *Chem. Rev.* **2020**, *120*, 6820.
[6] S. Sarkar, S. Roy, Y. Hou, S. Sun, J. Zhang, Y. Zhao, *ChemSusChem* **2021**, *14*, 3693.
[7] Y. Tian, G. Zeng, A. Rutt, T. Shi, H. Kim, J. Wang, J. Koettgen, Y. Sun, B. Ouyang, T. Chen, Z. Lun, Z. Rong, K. Persson, G. Ceder, *Chem. Rev.* **2021**, *121*, 1623.
[8] Z. Zhu, T. Jiang, M. Ali, Y. Meng, Y. Jin, Y. Cui, W. Chen, *Chem. Rev.* **2022**, *122*, 16610.
[9] D. Chao, W. Zhou, F. Xie, C. Ye, H. Li, M. Jaroniec, S. Z. Qiao, *Sci. Adv.* **2020**, *6*, eaba4098.
[10] J. Huang, P. Zhong, Y. Ha, D. H. Kwon, M. J. Crafton, Y. Tian, M. Balasubramanian, B. D. McCloskey, W. Yang, G. Ceder, *Nat. Energy* **2021**, *6*, 706.
[11] X. Wang, G. Pawar, Y. Li, X. Ren, M. Zhang, B. Lu, A. Banerjee, P. Liu, E. J. Dufek, J. G. Zhang, J. Xiao, J. Liu, Y. S. Meng, B. Liaw, *Nat. Mater.* **2020**, *19*, 1339.
[12] Q. Zheng, Y. Zhang, M. Montazerian, O. Gulbiten, J. C. Mauro, E. D. Zanotto, Y. Yue, *Chem. Rev.* **2019**, *119*, 7848.
[13] T. Rouxel, J. I. Jang, U. Ramamurty, *Prog. Mater. Sci.* **2021**, *121*, 100834.
[14] D. Möncke, B. Topper, A. G. Clare, *Rev. Miner. Geochem.* **2022**, *87*, 1039.
[15] R. Jiang, Y. Da, Z. Chen, X. Cui, X. Han, H. Ke, Y. Liu, Y. Chen, Y. Deng, W. Hu, *Adv. Energy Mater.* **2022**, *12*, 2101092.
[16] N. Ma, S. Horike, *Chem. Rev.* **2022**, *122*, 4163.
[17] a) F. Xiong, H. Tao, Y. Yue, *Front. Mater.* **2020**, *6*, 328; b) Y. Zhang, P. Wang, T. Zheng, D. Li, G. Li, Y. Yue, *Nano Energy* **2018**, *49*, 596; c) Z. A. Grady, C. J. Wilkinson, C. A. Randall, J. C. Mauro, *Front. Energy Res.* **2020**, *8*, 218; d) Z. Wei, D. Wang, X. Yang, C. Wang, G. Chen, F. Du, *Adv. Mater. Interfaces* **2018**, *5*, 1800639.
[18] J. Nai, X. Zhao, H. Yuan, X. Tao, L. Guo, *Nano Res.* **2021**, *14*, 2053.
[19] S. Yan, K. P. Abhilash, L. Tang, M. Yang, Y. Ma, Q. Xia, Q. Guo, H. Xia, *Small* **2019**, *15*, 1804371.
[20] Z. Xu, Y. Xia, *J. Mater. Chem. A* **2022**, *10*, 11854.
[21] J. Kang, X. Yang, Q. Hu, Z. Cai, L. M. Liu, L. Guo, *Chem. Rev.* **2023**, *123*, 8859.
[22] a) C. G. Lee, B. Cobb, A. Dodabalapur, *Appl. Phys. Lett.* **2010**, *97*, 203505; b) H. Hosono, *J. Non-Cryst. Solids* **2006**, *352*, 851.
[23] a) C. A. Angell, *Science* **1995**, *267*, 1924; b) J. Zhang, Y. Li, Z. Chen, Q. Liu, Q. Chen, M. Chen, *Energy Environ. Mater.* **2023**, https://doi.org/10.1002/eem2.12573.
[24] a) M. B. Dixit, N. Singh, J. P. Horwath, P. D. Shevchenko, M. Jones, E. A. Stach, T. S. Arthur, K. B. Hatzell, *Matter* **2020**, *3*, 2138; b) S. Gandi, V. S. Chidambara Swamy Vaddadi, S. S. Sripada Panda, N. K. Goona, S. R. Parne, M. Lakavat, A. Bhaumik, *J. Power Sources* **2022**, *521*, 230930.
[25] Z. Lin, X. Guo, H. Yu, *Nano Energy* **2017**, *41*, 646.
[26] a) C. Gao, Z. Jiang, S. Qi, P. Wang, L. R. Jensen, M. Johansen, C. K. Christensen, Y. Zhang, D. B. Ravnsbæk, Y. Yue, *Adv. Mater.* **2022**, *34*, 2110048; b) G. Jiang, C. Qu, F. Xu, E. Zhang, Q. Lu, X. Cai, S. Hausdorf, H. Wang, S. Kaskel, *Adv. Funct. Mater.* **2021**, *31*, 2104300; c) J. Yan, C. Gao, S. Qi, Z. Jiang, L. R. Jensen, H. Zhan, Y. Zhang, Y. Yue, *Nano Energy* **2022**, *103*, 107779.
[27] G. E. Möhl, E. Metwalli, P. Müller-Buschbaum, *ACS Energy Lett.* **2018**, *3*, 1525.
[28] D. J. Morales, S. Greenbaum, *Int. J. Mol. Sci.* **2020**, *21*, 3402.
[29] C. Yan, C. Lv, B.-E. Jia, L. Zhong, X. Cao, X. Guo, H. Liu, W. Xu, D. Liu, L. Yang, J. Liu, H. H. Hng, W. Chen, L. Song, S. Li, Z. Liu, Q. Yan, G. Yu, *J. Am. Chem. Soc.* **2022**, *144*, 11444.
[30] M. Kassem, T. Bounazef, D. Fontanari, A. Sokolov, M. Bokova, A. C. Hannon, E. Bychkov, *Inorg. Chem.* **2020**, *59*, 16410.
[31] C. K. Christensen, D. R. Sørensen, J. Hvam, D. B. Ravnsbæk, *Chem. Mater.* **2019**, *31*, 512.
[32] V. Ponce, D. E. Galvez-Aranda, J. M. Seminario, *J. Phys. Chem. C* **2017**, *121*, 12959.
[33] S. S. Sørensen, M. B. Østergaard, M. Stepniewska, H. Johra, Y. Yue, M. M. Smedskjaer, *ACS Appl. Mater. Interfaces* **2020**, *12*, 18893.
[34] Y. Wu, S. Wang, H. Li, L. Chen, F. Wu, *InfoMat* **2021**, *3*, 827.
[35] X. Ke, Y. Wang, G. Ren, C. Yuan, *Energy Storage Mater.* **2020**, *26*, 313.
[36] a) J. Gu, Z. Liang, J. Shi, Y. Yang, *Adv. Energy Mater.* **2023**, *13*, 2203153; b) C. D. Fincher, C. E. Athanasiou, C. Gilgenbach, M. Wang, B. W. Sheldon, W. C. Carter, Y.-M. Chiang, *Joule* **2022**, *6*, 2794.
[37] a) M. B. Preefer, J. H. Grebenkemper, C. E. Wilson, M. Everingham, J. A. Cooley, R. Seshadri, *ACS Appl. Mater. Interfaces* **2021**, *13*, 57567; b) E. L. Zhao, S. X. Zhao, X. Wu, J. W. Li, L. Q. Yu, C. W. Nan, G. Cao, *J. Materiomics* **2019**, *5*, 663; c) Y. Zhang, *Int. J. Appl. Glass Sci.* **2020**, *11*, 577; d) Y. Zhang, P. Wang, G. Li, J. Fan, C. Gao, Z. Wang, Y. Yue, *Nano Energy* **2019**, *57*, 592.

© 2023 The Authors. Small published by Wiley-VCH GmbH

16136829, 0, Downloaded from https://onlinelibrary.wiley.com/doi/10.1002/smll.202304270 by Aalborg University Library, Wiley Online Library on [06/12/2023]. See the Terms and Conditions (https://onlinelibrary.wiley.com/terms-and-conditions) on Wiley Online Library for rules of use; OA articles are governed by the applicable Creative Commons License

[38] a) A. Kato, M. Yamamoto, A. Sakuda, A. Hayashi, M. Tatsumisago, *ACS Appl. Energy Mater.* **2018**, *1*, 1002; b) B. S. Vishnugopi, M. T. Hasan, H. Zhou, P. P. Mukherjee, *ACS Energy Lett.* **2023**, *8*, 398.
[39] J. R. Rodriguez, Z. Qi, H. Wang, M. Y. Shalaginov, C. Goncalves, M. Kang, K. A. Richardson, J. Guerrero-Sanchez, M. G. Moreno-Armenta, V. G. Pol, *Nano Energy* **2020**, *68*, 104326.
[40] F. Kong, X. Liang, Y. Rao, X. Bi, R. Bai, X. Yu, D. Wang, Z. Chen, H. Jiang, C. Li, *Chem. Eng. J.* **2022**, *442*, 136228.
[41] L. David, R. Bhandavat, U. Barrera, G. Singh, *Nat. Commun.* **2016**, *7*, 10998.
[42] J. D. Esper, Y. Zhuo, M. K. S. Barr, T. Yokosawa, E. Spiecker, D. de Ligny, J. Bachmann, W. Peukert, S. Romeis, *Powder Technol.* **2020**, *363*, 218.
[43] S. H. Choi, S. J. Lee, H. J. Kim, S. B. Park, J. W. Choi, *J. Mater. Chem. A* **2018**, *6*, 6860.
[44] T. Zheng, H. Ge, J. Liu, G. Li, *J. Electron. Mater.* **2020**, *49*, 3819.
[45] T. Hakari, M. Nagao, A. Hayashi, M. Tatsumisago, *J. Power Sources* **2015**, *293*, 721.
[46] Z. Jiang, S. Qi, C. Gao, X. Li, Y. Zhang, Y. Yue, *J. Non-Cryst. Solids* **2022**, *576*, 121225.
[47] R. Wei, W. Xie, P. Li, S. Fu, X. Liu, X. Wang, S. Xu, J. Zhang, *J. Non-Cryst. Solids* **2022**, *578*, 121357.
[48] L. Q. Yu, S. X. Zhao, X. Wu, J. W. Li, E. L. Zhao, G. D. Wei, *J. Alloys Compd.* **2019**, *810*, 151938.
[49] J. Fan, Y. Zhang, G. Li, Y. Yue, *J. Non-Cryst. Solids* **2019**, *521*, 119491.
[50] R. Wei, X. Liu, Y. Tian, F. Huang, S. Xu, J. Zhang, *J. Am. Ceram. Soc.* **2023**, *106*, 330.
[51] P. Lv, H. Zhao, C. Gao, Z. Du, J. Wang, X. Liu, *J. Power Sources* **2015**, *274*, 542.
[52] F. P. McGrogan, T. Swamy, S. R. Bishop, E. Eggleton, L. Porz, X. Chen, Y. M. Chiang, K. J. Van Vliet, *Adv. Energy Mater.* **2017**, *7*, 1602011.
[53] K. Kaup, J. D. Bazak, S. H. Vajargah, X. Wu, J. Kulisch, G. R. Goward, L. F. Nazar, *Adv. Energy Mater.* **2020**, *10*, 1902783.
[54] F. Kong, L. Yi, S. Huang, X. Liang, Y. Rao, Z. Su, C. Li, H. Jiang, *Appl. Surf. Sci.* **2021**, *552*, 149495.
[55] a) M. Agostini, Y. Aihara, T. Yamada, B. Scrosati, J. Hassoun, *Solid State Ion.* **2013**, *244*, 48; b) S. S. Berbano, M. Mirsaneh, M. T. Lanagan, C. A. Randall, *Int. J. Appl. Glass Sci.* **2013**, *4*, 414; c) K. Minami, A. Hayashi, M. Tatsumisago, *Solid State Ionics* **2010**, *181*, 1505.
[56] Z. Chen, T. Du, R. Christensen, M. Bauchy, M. M. Smedskjaer, *ACS Energy Lett.* **2023**, *8*, 1969.
[57] C. Gao, J. Zhang, C. He, Y. Fu, T. Zhou, X. Li, S. Kang, L. Tan, Q. Jiao, S. Dai, Y. Yue, C. Lin, *Adv. Energy Mater.* **2023**, *13*, 2204386.
[58] M. Shigeno, K. Nagao, M. Deguchi, C. Hotehama, H. Kowada, A. Sakuda, A. Hayashi, M. Tatsumisago, *Solid State Ionics* **2019**, *339*, 114985.
[59] I. Mandal, S. Mannan, L. Wondraczek, N. N. Gosvami, A. R. Allu, N. M. A. Krishnan, *J. Phys. Chem. C* **2023**, *127*, 14636.
[60] a) X. Wu, S. X. Zhao, L. Q. Yu, J. W. Li, E. L. Zhao, C. W. Nan, *Electrochim. Acta* **2019**, *297*, 872; b) A. Kitajou, M. Hokazono, N. Taguchi, S. Tanaka, S. Okada, *J. Alloys Compd.* **2021**, *856*, 157449; c) H. Wang, J. Li, Y. Yin, J. Chen, L. Wang, P. Zhang, X. Lai, B. Yue, X. Hu, D. He, *J. Alloys Compd.* **2021**, *879*, 160293.
[61] P. Xue, C. Sun, H. Li, J. Liang, C. Lai, *Adv. Sci.* **2019**, *6*, 1900943.
[62] Y. Idota, T. Kubota, A. Matsufuji, Y. Maekawa, T. Miyasaka, *Science* **1997**, *276*, 1395.
[63] a) S. Y. Lim, W. Jang, S. Yun, W. S. Yoon, J. Y. Choi, D. Whang, *Mater. Res. Bull.* **2019**, *110*, 24; b) W. Cheng, F. Rechberger, G. Ilari, H. Ma, W. I. Lin, M. Niederberger, *Chem. Sci.* **2015**, *6*, 6908; c) J. Feng, H. Wang, Z. Hu, M. Zhang, X. Yang, R. Yuan, Y. Chai, *Ceram. Int.* **2019**, *45*, 13369.
[64] Q. Zhao, J. Liu, X. Li, Z. Xia, Q. Zhang, M. Zhou, W. Tian, M. Wang, H. Hu, Z. Li, W. Wu, H. Ning, M. Wu, *Chem. Eng. J.* **2019**, *369*, 215.
[65] Y. Jiang, D. Zhang, Y. Li, T. Yuan, N. Bahlawane, C. Liang, W. Sun, Y. Lu, M. Yan, *Nano Energy* **2014**, *4*, 23.
[66] G. D. Park, J.-K. Lee, Y. C. Kang, *Chem. Eng. J.* **2020**, *389*, 124350.
[67] a) W. Li, X. Guo, Y. Lu, L. Wang, A. Fan, M. Sui, H. Yu, *Energy Storage Mater.* **2017**, *7*, 203; b) L. Lin, X. Xu, C. Chu, M. K. Majeed, J. Yang, *Angew. Chem., Int. Ed.* **2016**, *55*, 14063; c) H. Orthner, H. Wiggers, M. Loewenich, S. Kilian, S. Bade, J. Lyubina, *J. Alloys Compd.* **2021**, *870*, 159315.
[68] J. H. Ku, J. H. Ryu, S. H. Kim, O. H. Han, S. M. Oh, *Adv. Funct. Mater.* **2012**, *22*, 3658.
[69] L. Wang, M. Shi, C. Yang, Y. Liu, J. Jiang, K. Dai, Z. Guo, C. Yan, *J. Alloys Compd.* **2019**, *804*, 243.
[70] J. Yu, H. Zhang, Y. Lin, J. Shen, Y. Xie, X. Huang, Q. Cai, H. Huang, *J. Energy Chem.* **2022**, *68*, 658.
[71] T. Liu, T. Yao, L. Li, L. Zhu, J. Wang, F. Li, H. Wang, *J. Colloid Interface Sci.* **2020**, *580*, 21.
[72] X. Sheng, Z. Zeng, C. Du, T. Shu, X. Meng, *J. Mater. Sci.* **2021**, *56*, 15258.
[73] Y. Kong, Z. Ma, Y. Ye, G. He, Y. Sun, X. Zuo, X. Xiao, J. Nan, *ACS Appl. Energy Mater.* **2018**, *1*, 7065.
[74] S. Huang, L. Zhang, L. Liu, L. Liu, J. Li, H. Hu, J. Wang, F. Ding, O. G. Schmidt, *Energy Storage Mater.* **2018**, *12*, 23.
[75] H. Wu, Z. Zhang, M. Qin, Q. Wang, Z. Cao, Y. Yu, B. Jia, X. Qu, *J. Am. Ceram. Soc.* **2020**, *103*, 2643.
[76] Z. Tu, G. Yang, H. Song, C. Wang, *ACS Appl. Mater. Interfaces* **2017**, *9*, 439.
[77] C. Deng, M. L. Lau, H. M. Barkholtz, H. Xu, R. Parrish, M. Xu, T. Xu, Y. Liu, H. Wang, J. G. Connell, K. A. Smith, H. Xiong, *Nanoscale* **2017**, *9*, 10757.
[78] S. X. Xu, W. Xu, L. J. Kong, Y. H. Zhang, *SN Appl. Sci.* **2020**, *2*, 199.
[79] L. Sun, Y. Zhang, D. Zhang, J. Liu, Y. Zhang, *Nano Res.* **2018**, *11*, 2733.
[80] J. Yang, Y. Wang, W. Li, L. Wang, Y. Fan, W. Jiang, W. Luo, Y. Wang, B. Kong, C. Selomulya, H. K. Liu, S. X. Dou, D. Zhao, *Adv. Mater.* **2017**, *29*, 1700523.
[81] H. Cheng, D. Li, B. Xu, Y. Wei, H. Wang, B. Jiang, X. Liu, H. Xu, Y. Huang, *Energy Storage Mater.* **2022**, *53*, 305.
[82] J. Cheng, K. D. Fong, K. A. Persson, *J. Mater. Chem. A* **2022**, *10*, 22245.
[83] T. Feng, T. Zhao, N. Zhang, Y. Duan, L. Li, F. Wu, R. Chen, *Adv. Funct. Mater.* **2022**, *32*, 2202766.
[84] A. Dutta, R. A. Wong, W. Park, K. Yamanaka, T. Ohta, Y. Jung, H. R. Byon, *Nat. Commun.* **2018**, *9*, 680.
[85] T. Okumura, S. Taminato, Y. Miyazaki, M. Kitamura, T. Saito, T. Takeuchi, H. Kobayashi, *ACS Appl. Energy Mater.* **2020**, *3*, 3220.
[86] J. Heo, S. K. Jung, I. Hwang, S. P. Cho, D. Eum, H. Park, J. H. Song, S. Yu, K. Oh, G. Kwon, T. Hwang, K. H. Ko, K. Kang, *Nat. Energy* **2023**, *8*, 30.
[87] J. Sheng, Q. Li, Q. Wei, P. Zhang, Q. Wang, F. Lv, Q. An, W. Chen, L. Mai, *Nano Res.* **2014**, *7*, 1604.
[88] T. Liu, Y. Liu, C. Niu, Z. Chao, *ChemElectroChem* **2022**, *9*, 202101493.
[89] K. Nagao, A. Hayashi, M. Deguchi, H. Tsukasaki, S. Mori, M. Tatsumisago, *J. Power Sources* **2017**, *348*, 1.
[90] K. Lemoine, L. Zhang, J.-M. Grenèche, A. Hémon-Ribaud, M. Leblanc, A. Guiet, C. Galven, J. M. Tarascon, V. Maisonneuve, J. Lhoste, *J. Phys. Chem. C* **2019**, *123*, 21386.
[91] W. Fan, M. Jiang, G. Liu, W. Weng, J. Yang, X. Yao, *ACS Appl. Mater. Interfaces* **2022**, *14*, 17594.
[92] F. Kong, D. Sun, Y. Rao, R. Zhang, Z. Chen, D. Wang, X. Yu, H. Jiang, C. Li, *Appl. Surf. Sci.* **2022**, *573*, 151490.
[93] J. Cheng, E. Sivonxay, K. A. Persson, *ACS Appl. Mater. Interfaces* **2020**, *12*, 35748.

© 2023 The Authors. Small published by Wiley-VCH GmbH

16136829, 0, Downloaded from https://onlinelibrary.wiley.com/doi/10.1002/smll.202304270 by Aalborg University Library, Wiley Online Library on [06/12/2023]. See the Terms and Conditions (https://onlinelibrary.wiley.com/terms-and-conditions) on Wiley Online Library for rules of use; OA articles are governed by the applicable Creative Commons License

[94] a) F. Mattelaer, P. M. Vereecken, J. Dendooven, C. Detavernier, *Adv. Mater. Interfaces* **2017**, *4*, 1601237; b) Y. J. Lim, S. M. Lee, H. Lim, B. Moon, K. S. Han, J. H. Kim, J. H. Song, J. S. Yu, W. Cho, M. S. Park, *Electrochim. Acta* **2018**, *282*, 311.
[95] X. Yao, N. Huang, F. Han, Q. Zhang, H. Wan, J. P. Mwizerwa, C. Wang, X. Xu, *Adv. Energy Mater.* **2017**, *7*, 1602923.
[96] a) L. Lodovico, S. Milad Hosseini, A. Varzi, S. Passerini, *Energy Technol.* **2019**, *7*, 1801013; b) X. Meng, D. J. Comstock, T. T. Fister, J. W. Elam, *ACS Nano* **2014**, *8*, 10963.
[97] R. Sun, Y. Bai, M. Luo, M. Qu, Z. Wang, W. Sun, K. Sun, *ACS Nano* **2021**, *15*, 739.
[98] S. Deng, Y. Yan, L. Wei, T. Li, X. Su, X. Yang, Z. Li, M. Wu, *ACS Appl. Energy Mater.* **2019**, *2*, 1266.
[99] Z. Liu, X. Zheng, S. L. Luo, S. Q. Xu, N. Y. Yuan, J. N. Ding, *J. Mater. Chem. A* **2016**, *4*, 13395.
[100] J. Yu, J. Xiao, A. Li, Z. Yang, L. Zeng, Q. Zhang, Y. Zhu, L. Guo, *Angew. Chem., Int. Ed.* **2020**, *59*, 13071.
[101] S. Liu, Y. Li, C. Zhang, X. Chen, Z. Wang, F. Cui, X. Yang, W. Yue, *Electrochim. Acta* **2020**, *332*, 135458.
[102] K. Chen, G. Zhang, L. Xiao, P. Li, W. Li, Q. Xu, J. Xu, *Small Methods* **2021**, *5*, 2001056.
[103] R. Gao, X. Liang, P. Yin, J. Wang, Y. L. Lee, Z. Hu, X. Liu, *Nano Energy* **2017**, *41*, 535.
[104] J. Yang, D. Ma, Y. Li, P. Zhang, H. Mi, L. Deng, L. Sun, X. Ren, *J. Power Sources* **2017**, *360*, 215.
[105] B. Wang, F. Yuan, J. Wang, D. Zhang, W. Li, Q. Wang, H. Sun, *Electrochim. Acta* **2020**, *354*, 136627.
[106] S. K. Yerranuka, V. K. Katta, N. K. Katari, S. Rajesh Kumar, D. P. Dutta, B. R. Ravuri, *Energy Technol.* **2022**, *10*, 2100343.
[107] S. Gandi, W. Mekprasart, W. Pecharapa, D. P. Dutta, C. K. Jayasankar, B. R. Ravuri, *Mater. Chem. Phys.* **2020**, *242*, 122568.
[108] S. Gandi, S. R. Chinta, P. Ghoshal, B. R. Ravuri, *J. Non-Cryst. Solids* **2019**, *506*, 80.
[109] T. Honma, T. Togashi, H. Kondo, T. Komatsu, H. Yamauchi, A. Sakamoto, T. Sakai, *APL Mater.* **2013**, *1*, 052101.
[110] X. Chi, Y. Zhang, F. Hao, S. Kmiec, H. Dong, R. Xu, K. Zhao, Q. Ai, T. Terlier, L. Wang, L. Zhao, L. Guo, J. Lou, H. L. Xin, S. W. Martin, Y. Yao, *Nat. Commun.* **2022**, *13*, 2854.
[111] I. Mandal, S. Chakraborty, M. Ghosh, K. K. Dey, K. Annapurna, A. R. Allu, *Front. Mater.* **2022**, *8*, 802379.
[112] C. Calahoo, J. Petrovic, Q. H. Le, U. Werner-Zwanziger, J. Zwanziger, L. Wondraczek, *Front. Mater.* **2019**, *6*, 165.
[113] S. R. Keshri, S. Ganisetti, R. Kumar, A. Gaddam, K. Illath, T. G. Ajithkumar, S. Balaji, K. Annapurna, N. Nasani, N. M. A. Krishnan, A. R. Allu, *Inorg. Chem.* **2021**, *60*, 12893.
[114] A. Dive, Y. Zhang, Y. Yao, S. W. Martin, S. Banerjee, *Solid State Ionics* **2019**, *338*, 177.
[115] a) A. Nasu, T. Inaoka, F. Tsuji, K. Motohashi, A. Sakuda, M. Tatsumisago, A. Hayashi, *ACS Appl. Mater. Interfaces* **2022**, *14*, 24480; b) F. Tsuji, A. Nasu, C. Hotehama, A. Sakuda, M. Tatsumisago, A. Hayashi, *Mater. Adv.* **2021**, *2*, 1676.
[116] I. Mandal, S. Chakraborty, K. Jayanthi, M. Ghosh, K. K. Dey, K. Annapurna, J. Mukhopadhyay, A. D. Sharma, A. R. Allu, *J. Phys. Chem. C* **2022**, *126*, 3276.
[117] I. Mandal, S. Chakraborty, K. Annapurna, A. Das Sharma, J. Mukhopadhyay, A. R. Allu, *J. Alloys Compd.* **2021**, *885*, 160952.
[118] K. H. Sadok, M. Haouari, O. Gallot-Lavallée, H. Ben Ouada, *J. Alloys Compd.* **2019**, *778*, 878.
[119] S. W. Martin, R. Christensen, G. Olson, J. Kieffer, W. Wang, *J. Phys. Chem. C* **2019**, *123*, 5853.
[120] A. Paraskiva, M. Bokova, E. Bychkov, *Solid State Ionics* **2017**, *299*, 2.
[121] N. Tanibata, K. Noi, A. Hayashi, M. Tatsumisago, *Solid State Ionics* **2018**, *320*, 193.
[122] Y. Zhao, F. Tong, C. Fan, S. Yu, B. Han, J. Gao, Y. Lou, P. Jiang, Z. Wang, *Bull. Mater. Sci.* **2020**, *43*, 75.
[123] S. Nakata, T. Togashi, T. Honma, T. Komatsu, *J. Non-Cryst. Solids* **2016**, *450*, 109.
[124] A. Ibrahim, K. Kubo, S. Watanabe, S. Shiba, I. Khan, B. Zhang, Z. Homonnay, E. Kuzmann, L. Pavić, A. Santić, A. S. Ali, M. Y. Hassaan, S. Kubuki, *J. Alloys Compd.* **2023**, *930*, 167366.
[125] L. Zhou, P. Jiao, L. Fang, L. Liu, Z. Hao, H. Wang, Y. M. Kang, K. Zhang, J. Chen, *ACS Nano* **2021**, *15*, 13486.
[126] L. Shi, Y. Li, F. Zeng, S. Ran, C. Dong, S. Y. Leu, S. T. Boles, K. H. Lam, *Chem. Eng. J.* **2019**, *356*, 107.
[127] a) F. Legrain, J. Sottmann, K. Kotsis, S. Gorantla, S. Sartori, S. Manzhos, *J. Phys. Chem. C* **2015**, *119*, 13496; b) Y. Li, Y. S. Hu, H. Li, L. Chen, X. Huang, *J. Mater. Chem. A* **2016**, *4*, 96; c) W. Wang, H. Huang, B. Wang, C. Qian, P. Li, J. Zhou, Z. Liang, C. Yang, S. Guo, *Sci. Bull.* **2019**, *64*, 1634.
[128] a) P. Lu, Y. Sun, H. Xiang, X. Liang, Y. Yu, *Adv. Energy Mater.* **2018**, *8*, 1702434; b) J. Han, I. Johnson, Z. Lu, A. Kudo, M. Chen, *Nano Lett.* **2021**, *21*, 6504.
[129] D. Li, J. Zhou, X. Chen, H. Song, *ACS Appl. Mater. Interfaces* **2016**, *8*, 30899.
[130] C. Wang, D. Wang, X. Ma, H. Qin, M. Liu, Y. Yan, B. Zhang, X. Ou, *Adv. Funct. Mater.* **2022**, *32*, 2204687.
[131] X. Zhang, J. Wang, X. Wang, Y. Li, Y. Zhao, Z. Bakenov, G. Li, *Appl. Surf. Sci.* **2021**, *567*, 150862.
[132] J. Zhu, D. Deng, *J. Phys. Chem. C* **2015**, *119*, 21323.
[133] R. Sun, J. Gao, G. Wu, P. Liu, W. Guo, H. Zhou, J. Ge, Y. Hu, Z. Xue, H. Li, P. Cui, X. Zheng, Y. Wu, G. Zhang, X. Hong, *Cell Rep. Phys. Sci.* **2020**, *1*, 100118.
[134] W. Zhang, J. Peng, W. Hua, Y. Liu, J. Wang, Y. Liang, W. Lai, Y. Jiang, Y. Huang, W. Zhang, H. Yang, Y. Yang, L. Li, Z. Liu, L. Wang, S.-L. Chou, *Adv. Energy Mater.* **2021**, *11*, 2100757.
[135] S. Huang, L. Liu, Y. Zheng, Y. Wang, D. Kong, Y. Zhang, Y. Shi, L. Zhang, O. G. Schmidt, H. Y. Yang, *Adv. Mater.* **2018**, *30*, 1706637.
[136] Z. L. Xu, S. Yao, J. Cui, L. Zhou, J. K. Kim, *Energy Storage Mater.* **2017**, *8*, 10.
[137] F. H. Du, L. Zhang, Y. C. Tang, S. Q. Li, Y. Huang, L. Dong, Q. Li, H. Liu, D. Wang, Y. Wang, *Adv. Mater. Interfaces* **2022**, *9*, 2102158.
[138] J. Rahmatinejad, X. Liu, X. Zhang, B. Raisi, Z. Ye, *J. Energy Chem.* **2022**, *75*, 240.
[139] X. Li, S. Guo, K. Jiang, Y. Qiao, M. Ishida, H. Zhou, *ACS Appl. Mater. Interfaces* **2018**, *10*, 16.
[140] H. Ye, L. Wang, S. Deng, X. Zeng, K. Nie, P. N. Duchesne, B. Wang, S. Liu, J. Zhou, F. Zhao, N. Han, P. Zhang, J. Zhong, X. Sun, Y. Li, Y. Li, J. Lu, *Adv. Energy Mater.* **2017**, *7*, 1601602.
[141] K. Zhu, X. Wang, J. Liu, S. Li, H. Wang, L. Yang, S. Liu, T. Xie, *ACS Sustainable Chem. Eng.* **2017**, *5*, 8025.
[142] Z. Zhao, C. Li, Z. Liu, D. Li, *Int. J. Hydrogen Energy* **2021**, *46*, 26457.
[143] a) Y. Zhang, L. Zhou, F. Xiong, H. Tang, Q. An, L. Mai, *Inorg. Chem. Front.* **2018**, *5*, 2756; b) S. Dou, X. Li, L. Fan, D. Xiong, H. M. Kheimeh Sari, B. Yan, W. Liu, J. Li, J. Xu, D. Li, X. Sun, *Electrochim. Acta* **2019**, *316*, 236.
[144] X. Zhu, X. Jiang, X. Liu, L. Xiao, X. Ai, H. Yang, Y. Cao, *Ceram. Int.* **2017**, *43*, 9630.
[145] Y. Zhu, J. Zhao, J. Chen, J. Xu, *J. Appl. Electrochem.* **2020**, *50*, 513.
[146] Y. M. Xing, X. H. Zhang, D. H. Liu, W. H. Li, L. N. Sun, H. B. Geng, J. P. Zhang, H. Y. Guan, X. L. Wu, *ChemElectroChem* **2017**, *4*, 1395.
[147] B. Long, Z. Qiao, J. Zhang, S. Zhang, M. S. Balogun, J. Lu, S. Song, Y. Tong, *J. Mater. Chem. A* **2019**, *7*, 11370.
[148] J. Yu, H. Zhang, E. Olsson, T. Yu, Z. Liu, S. Zhang, X. Huang, W. Li, Q. Cai, *J. Mater. Chem. A* **2021**, *9*, 12029.
[149] J. Yang, J. Li, T. Wang, P. H. L. Notten, H. Ma, Z. Liu, C. Wang, G. Wang, *Chem. Eng. J.* **2021**, *407*, 127169.

© 2023 The Authors. Small published by Wiley-VCH GmbH

16136829, 0, Downloaded from https://onlinelibrary.wiley.com/doi/10.1002/smll.202304270 by Aalborg University Library, Wiley Online Library on [06/12/2023]. See the Terms and Conditions (https://onlinelibrary.wiley.com/terms-and-conditions) on Wiley Online Library for rules of use; OA articles are governed by the applicable Creative Commons License

[150] a) W. Zhao, M. Li, Y. Qi, Y. Tao, Z. Shi, Y. Liu, J. Cheng, *J. Colloid Interface Sci.* **2021**, *586*, 404; b) Y. Zhao, A. Manthiram, *Chem. Commun.* **2015**, *51*, 13205.
[151] K. H. Nam, C. M. Park, *J. Power Sources* **2019**, *433*, 126639.
[152] M. Wang, A. Peng, H. Xu, Z. Yang, L. Zhang, J. Zhang, H. Yang, J. Chen, Y. Huang, X. Li, *J. Power Sources* **2020**, *469*, 228414.
[153] X. Yang, R.-Y. Zhang, J. Zhao, Z. X. Wei, D. X. Wang, X. F. Bie, Y. Gao, J. Wang, F. Du, G. Chen, *Adv. Energy Mater.* **2018**, *8*, 1701827.
[154] Y. Xu, M. Zhou, C. Zhang, C. Wang, L. Liang, Y. Fang, M. Wu, L. Cheng, Y. Lei, *Nano Energy* **2017**, *38*, 304.
[155] a) F. Bella, A. B. Muñoz-García, G. Meligrana, A. Lamberti, M. Destro, M. Pavone, C. Gerbaldi, *Nano Res.* **2017**, *10*, 2891; b) M. Zhou, Y. Xu, C. Wang, Q. Li, J. Xiang, L. Liang, M. Wu, H. Zhao, Y. Lei, *Nano Energy* **2017**, *31*, 514.
[156] a) S. Osman, C. Peng, J. Shen, F. Li, W. Huang, J. Liu, J. Liu, D. Xue, M. Zhu, *Nano Energy* **2022**, *100*, 107481; b) E. Uchaker, Y. Z. Zheng, S. Li, S. L. Candelaria, S. Hu, G. Z. Cao, *J. Mater. Chem. A* **2014**, *2*, 18208.
[157] D. Chao, R. DeBlock, C. H. Lai, Q. Wei, B. Dunn, H. J. Fan, *Adv. Mater.* **2021**, *33*, 2103736.
[158] Z. Qin, C. Lv, J. Pei, C. Yan, Y. Hu, G. Chen, *Small* **2020**, *16*, 1906214.
[159] a) W. Li, S. Hu, X. Luo, Z. Li, X. Sun, M. Li, F. Liu, Y. Yu, *Adv. Mater.* **2017**, *29*, 1605820; b) C. Zhang, X. Wang, Q. Liang, X. Liu, Q. Weng, J. Liu, Y. Yang, Z. Dai, K. Ding, Y. Bando, J. Tang, D. Golberg, *Nano Lett.* **2016**, *16*, 2054.
[160] Y. Zhang, P. Wang, Y. Yin, N. Liu, N. Song, L. Fan, N. Zhang, K. Sun, *Carbon* **2019**, *150*, 378.
[161] Z. Li, J. Feng, H. Hu, Y. Dong, H. Ren, W. Wu, Z. Hu, M. Wu, *J. Mater. Chem. A* **2018**, *6*, 18920.
[162] I. Y. Choi, C. Jo, W. G. Lim, J. C. Han, B. G. Chae, C. G. Park, J. Lee, J. K. Kim, *ACS Nano* **2019**, *13*, 6513.
[163] S. Sinha, P. N. Didwal, D. K. Nandi, R. Verma, J. Y. Cho, S. H. Kim, C. J. Park, J. Heo, *Small* **2019**, *15*, 1900595.
[164] a) Y. Liu, Y. Xu, X. Han, C. Pellegrinelli, Y. Zhu, H. Zhu, J. Wan, A. C. Chung, O. Vaaland, C. Wang, L. Hu, *Nano Lett.* **2012**, *12*, 5664; b) X. Zhao, M. Luo, K. Peng, Z. Zhang, B. Cheng, B. Wang, C. Zhu, X. Yan, K. Shi, *ACS Appl. Mater. Interfaces* **2021**, *13*, 57442; c) L. Zhang, L. Yu, O. L. Li, S. Y. Choi, G. Saeed, D. Lee, K. H. Kim, *ACS Appl. Energy Mater.* **2022**, *5*, 5954.
[165] a) Y. Fang, L. Xiao, J. Qian, X. Ai, H. Yang, Y. Cao, *Nano Lett.* **2014**, *14*, 3539; b) Z. Zhang, Y. Han, J. Xu, J. Ma, X. Zhou, J. Bao, *ACS Appl. Energy Mater.* **2018**, *1*, 4395.
[166] S. Y. Lim, J. H. Lee, S. Kim, J. Shin, W. Choi, K. Y. Chung, D. S. Jung, J. W. Choi, *ACS Energy Lett.* **2017**, *2*, 998.
[167] F. Xiong, Q. An, L. Xia, Y. Zhao, L. Mai, H. Tao, Y. Yue, *Nano Energy* **2019**, *57*, 608.
[168] X. H. Ma, F. Zhang, Y. Y. Wei, J. H. Zhou, J. Wang, W. Jia, Z. F. Zi, J. M. Dai, *J. Alloys Compd.* **2018**, *768*, 181.
[169] Y. Fang, J. Zhang, F. Zhong, X. Feng, W. Chen, X. Ai, H. Yang, Y. Cao, *CCS Chem.* **2021**, *3*, 2428.
[170] A. Kitajou, H. Momida, T. Yamashita, T. Oguchi, S. Okada, *ACS Appl. Energy Mater.* **2019**, *2*, 5968.
[171] A. Nasu, M. Otoyama, A. Sakuda, A. Hayashi, M. Tatsumisago, *Chem. Lett.* **2019**, *48*, 288.
[172] Y. Zhou, T. Chen, J. Zhang, Y. Liu, P. Ren, *Chin. J. Chem.* **2017**, *35*, 1294.
[173] T. Liu, Y. Duan, G. Zhang, M. Li, Y. Feng, J. Hu, J. Zheng, J. Chen, F. Pan, *J. Mater. Chem. A* **2016**, *4*, 4479.
[174] J. Zhou, Y. Yang, Y. Zhang, S. Duan, X. Zhou, W. Sun, S. Xu, *Angew. Chem., Int. Ed.* **2021**, *60*, 10129.
[175] D. Zhao, L. Wang, M. Qiu, N. Zhang, *ACS Appl. Energy Mater.* **2021**, *4*, 7219.
[176] a) Y. Sun, Q. Wu, Y. Wang, C. Li, X. Liang, H. Xiang, *J. Power Sources* **2021**, *512*, 230530; b) R. Guo, X. Liu, B. Wen, F. Liu, J. Meng, P. Wu, J. Wu, Q. Li, L. Mai, *Nanomicro Lett.* **2020**, *12*, 148.
[177] B. Wang, F. Yuan, Q. Yu, W. Li, H. Sun, L. Zhang, D. Zhang, Q. Wang, F. Lai, W. Wang, *Energy Storage Mater.* **2021**, *38*, 329.
[178] M. Huang, B. Xi, L. Mi, Z. Zhang, W. Chen, J. Feng, S. Xiong, *Small* **2022**, *18*, 2107819.
[179] Q. Li, Y. Sun, K. Shi, J. Li, W. Jian, W. Zhang, H. Li, M. Wu, H. Dang, Q. Liu, *ACS Appl. Energy Mater.* **2022**, *5*, 14401.
[180] Q. Yu, B. Wang, J. Hu, G. Suo, Q. Wang, H. Mei, K. Xi, S. Lu, W. Wang, J. Zhang, *J. Power Sources* **2021**, *506*, 230117.
[181] X. Niu, Y. Zhang, L. Tan, Z. Yang, J. Yang, T. Liu, L. Zeng, Y. Zhu, L. Guo, *Energy Storage Mater.* **2019**, *22*, 160.
[182] D. Yu, Q. Li, W. Zhang, S. Huang, *Small* **2022**, *18*, 2202750.
[183] J. B. Lim, M. Kim, S. K. Park, *Appl. Surf. Sci.* **2022**, *602*, 154332.
[184] R. Li, J. Wu, J. He, X. Li, Y. W. Mai, Y. Chen, X. Li, *Composites, Part B* **2022**, *243*, 110132.
[185] a) T. Michlik, M. Schmid, A. Rosin, T. Gerdes, R. Moos, *Batteries* **2018**, *4*, 12; b) M. Schmid, M. Willert-Porada, *Electrochim. Acta* **2018**, *260*, 246.
[186] X. Wu, F. Chen, N. Zhang, A. Qaseem, R. L. Johnston, *J. Mater. Chem. A* **2016**, *4*, 3527.
[187] J. Zheng, G. Zhu, X. Liu, H. Xie, Y. Lin, Y. Zeng, Y. Zhang, A. N. Gandi, Z. Qi, Z. Wang, H. Liang, *ACS Energy Lett.* **2022**, *7*, 4443.
[188] W. Li, Q. Zhang, Z. Yang, H. Ji, T. Wu, H. Wang, Z. Cai, C. Xie, Y. Li, H. Wang, *Small* **2022**, *18*, 2205667.
[189] a) J. Zheng, Y. Wu, H. Xie, Y. Zeng, W. Liu, A. N. Gandi, Z. Qi, Z. Wang, H. Liang, *ACS Nano* **2023**, *17*, 337; b) T. Xin, Y. Wang, Q. Xu, J. Shang, X. Yuan, W. Song, J. Liu, *ACS Appl. Energy Mater.* **2022**, *5*, 2290.
[190] S. Deng, Z. Yuan, Z. Tie, C. Wang, L. Song, Z. Niu, *Angew. Chem., Int. Ed.* **2020**, *59*, 22002.
[191] L. Ou, Z. Liu, Y. Zhou, H. Ou, J. Zhu, X. Cao, G. Fang, J. Zhou, S. Liang, *Chem. Eng. J.* **2021**, *426*, 131868.
[192] Y. Wu, J. Fee, Z. Tobin, A. Shirazi-Amin, P. Kerns, S. Dissanayake, A. Mirich, S. L. Suib, *ACS Appl. Energy Mater.* **2020**, *3*, 1627.
[193] C. Li, M. Li, H. Xu, F. Zhao, S. Gong, H. Wang, J. Qi, Z. Wang, X. Fan, W. Peng, J. Liu, *J. Colloid Interface Sci.* **2022**, *623*, 277.
[194] S. Zhang, H. Zhang, S. Li, L. Li, S. Zhang, Z. Liu, *J. Power Sources* **2022**, *543*, 231825.
[195] a) X. Wang, Y. Li, S. Wang, F. Zhou, P. Das, C. Sun, S. Zheng, Z. S. Wu, *Adv. Energy Mater.* **2020**, *10*, 2000081; b) Y. Zhang, J. Qin, M. Batmunkh, W. Li, H. Fu, L. Wang, M. Al-Mamun, D. Qi, P. Liu, S. Zhang, Y. L. Zhong, *Small* **2022**, *18*, 2105761.
[196] a) H. Tong, T. Li, J. Liu, D. Gong, J. Xiao, L. Shen, B. Ding, X. Zhang, *Energy Technol.* **2021**, *9*, 2000769; b) Y. Cai, R. Chua, S. Huang, H. Ren, M. Srinivasan, *Chem. Eng. J.* **2020**, *396*, 125221; c) S. Bi, Y. Wu, A. Cao, J. Tian, S. Zhang, Z. Niu, *Mater. Today Energy* **2020**, *18*, 100548.
[197] N. Li, G. Qu, X. Zhang, S. Zhao, C. Wang, G. Zhao, P. Hou, X. Xu, *Chin. Chem. Lett.* **2022**, *33*, 3272.
[198] S. Zhang, Z. Liu, L. Li, Y. Tang, S. Li, H. Huang, H. Zhang, *J. Mater. Chem. A* **2021**, *9*, 18488.
[199] B. Ju, H. J. Song, H. Yoon, D. W. Kim, *Chem. Eng. J.* **2021**, *420*, 130528.
[200] Y. Luo, L. Wei, H. Geng, Y. Zhang, Y. Yang, C. C. Li, *ACS Appl. Mater. Interfaces* **2020**, *12*, 11753.
[201] W. Niu, Y. Yang, *ACS Appl. Energy Mater.* **2018**, *1*, 2440.
[202] H. Zou, G. Li, L. Duan, Z. Kou, J. Wang, *Appl. Catal., B* **2019**, *259*, 118100.
[203] R. Li, Q. Li, L. Xiao, X. Bai, S. Ji, J. Zhang, M. An, P. Yang, *Mater. Today Energy* **2021**, *22*, 100882.
[204] Z. H. Guo, C. Yue, K. Q. Ou, L. F. Wu, Q. Y. Lv, J. Y. Lin, P. R. Chen, J. H. Liu, S. Huang, J. K. Li, J. L. Song, *Energy Technol.* **2022**, *10*, 2100940.

© 2023 The Authors. Small published by Wiley-VCH GmbH

16136829, 0, Downloaded from https://onlinelibrary.wiley.com/doi/10.1002/smll.202304270 by Aalborg University Library, Wiley Online Library on [06/12/2023]. See the Terms and Conditions (https://onlinelibrary.wiley.com/terms-and-conditions) on Wiley Online Library for rules of use; OA articles are governed by the applicable Creative Commons License

[205] D. S. Pan, P. Chen, L. L. Zhou, J. H. Liu, Z. H. Guo, J. L. Song, *J. Power Sources* **2021**, *498*, 229859.
[206] W. Zhao, T. Xu, T. Li, Y. Wang, H. Liu, J. Feng, S. Ding, Z. Li, M. Wu, *Small* **2018**, *14*, 1802829.
[207] S. Li, X. Yang, S. Yang, Q. Gao, S. Zhang, X. Yu, Y. Fang, S. Yang, X. Cai, *J. Mater. Chem. A* **2020**, *8*, 5601.
[208] M. I. Ojovan, W. E. Lee, *Metall. Mater. Trans. A* **2011**, *42*, 837.
[209] I. Pignatelli, A. Kumar, M. Bauchy, G. Sant, *Langmuir* **2016**, *32*, 4434.
[210] H. Liu, T. Zhang, N. M. Anoop Krishnan, M. M. Smedskjaer, J. V. Ryan, S. Gin, M. Bauchy, *NPJ Mater. Degrad.* **2019**, *3*, 32.
[211] D. Chen, D. Tao, X. Ren, F. Wen, T. Li, Z. Chen, Y. Cao, F. Xu, *ACS Nano* **2022**, *16*, 20510.
[212] M. Mao, C. Yang, Z. Lin, Y. Tong, Q. Zhang, L. Gu, L. Hong, L. Suo, Y. S. Hu, H. Li, X. Huang, L. Chen, *JACS Au* **2021**, *1*, 1266.
[213] D. Kim, J. H. Ryu, *Electron. Mater. Lett.* **2019**, *15*, 415.
[214] T. S. Arthur, K. Kato, J. Germain, J. Guo, P. A. Glans, Y. S. Liu, D. Holmes, X. Fan, F. Mizuno, *Chem. Commun.* **2015**, *51*, 15657.
[215] H. Chen, H. Xu, B. Li, Z. Li, K. Zhang, J. Zou, Z. Hu, R. M. Laine, *Appl. Surf. Sci.* **2022**, *598*, 153768.
[216] a) F. Legrain, O. I. Malyi, S. Manzhos, *Comput. Mater. Sci.* **2014**, *94*, 214; b) F. Legrain, O. Malyi, S. Manzhos, *J. Power Sources* **2015**, *278*, 197.
[217] a) T. Yamanaka, A. Hayashi, A. Yamauchi, M. Tatsumisago, *Solid State Ionics* **2014**, *262*, 601; b) M. Heere, A. L. Hansen, S. Payandeh, N. Aslan, G. Gizer, M. H. Sørby, B. C. Hauback, C. Pistidda, M. Dornheim, W. Lohstroh, *Sci. Rep.* **2020**, *10*, 9080.
[218] Z. Lin, M. Mao, C. Yang, Y. Tong, Q. Li, J. Yue, G. Yang, Q. Zhang, L. Hong, X. Yu, L. Gu, Y. S. Hu, H. Li, X. Huang, L. Suo, L. Chen, *Sci. Adv.* **2021**, *7*, eabg6314.
[219] A. P. Vijaya Kumar Saroja, A. Arjunan, K. Muthusamy, V. Balasubramanian, R. Sundara, *J. Alloys Compd.* **2020**, *830*, 154693.
[220] M. Chiku, H. Takeda, S. Matsumura, E. Higuchi, H. Inoue, *ACS Appl. Mater. Interfaces* **2015**, *7*, 24385.
[221] M. Lu, L. An, J. Yin, J. Jin, R. Yang, B. Huang, Y. Hu, Y. Q. Zhao, P. Xi, *J. Mater. Chem. A* **2022**, *10*, 19757.
[222] D. Yang, Y. Song, M. Y. Zhang, Z. Qin, J. Liu, X. X. Liu, *Angew. Chem., Int. Ed.* **2022**, *61*, e202207711.
[223] L. Frentzel-Beyme, M. Kloß, R. Pallach, S. Salamon, H. Moldenhauer, J. Landers, H. Wende, J. Debus, S. Henke, *J. Mater. Chem. A* **2019**, *7*, 985.
[224] T. To, S. S. Sørensen, M. Stepniewska, A. Qiao, L. R. Jensen, M. Bauchy, Y. Yue, M. M. Smedskjaer, *Nat. Commun.* **2020**, *11*, 2593.
[225] R. S. K. Madsen, A. Qiao, J. Sen, I. Hung, K. Chen, Z. Gan, S. Sen, Y. Yue, *Science* **2020**, *367*, 1473.
[226] Y. Seino, M. Nakagawa, M. Senga, H. Higuchi, K. Takada, T. Sasaki, *J. Mater. Chem. A* **2015**, *3*, 2756.
[227] a) A. Das, S. Sahu, M. Mohapatra, S. Verma, A. J. Bhattacharyya, S. Basu, *Mater. Today Energy* **2022**, *29*, 101118; b) K. Uchida, T. Ohkubo, F. Utsuno, K. Yazawa, *ACS Appl. Mater. Interfaces* **2021**, *13*, 37071.
[228] J. G. Smith, D. J. Siegel, *Nat. Commun.* **2020**, *11*, 1483.
[229] a) S. Qi, X. Li, Z. Jiang, J. Zhang, Z. Shan, Y. Zhang, *J. Am. Ceram. Soc.* **2022**, *105*, 1001; b) J. D. Esper, F. Maußner, S. Romeis, Y. Zhuo, M. K. S. Barr, T. Yokosawa, E. Spiecker, J. Bachmann, W. Peukert, *Energy Technol.* **2022**, *10*, 2200072; c) S. Liu, W. Tang, J. Ma, Y. Zhang, Y. Yue, *ACS Appl. Energy Mater.* **2020**, *3*, 9760.
[230] a) Z. Zheng, H.-H. Wu, H. Liu, Q. Zhang, X. He, S. Yu, V. Petrova, J. Feng, R. Kostecki, P. Liu, D.-L. Peng, M. Liu, M. S. Wang, *ACS Nano* **2020**, *14*, 9545; b) T. He, J. Feng, J. Ru, Y. Feng, R. Lian, J. Yang, *ACS Nano* **2019**, *13*, 830.
[231] a) P. Yan, L. Ji, X. Liu, Q. Guan, J. Guo, Y. Shen, H. Zhang, W. Wei, X. Cui, Q. Xu, *Nano Energy* **2021**, *86*, 106139; b) H. Chen, G. Ke, X. Wu, W. Li, Y. Li, H. Mi, L. Sun, Q. Zhang, C. He, X. Ren, *Chem. Eng. J.* **2021**, *406*, 126775.
[232] N. Li, J. Peng, P. Zhang, Y. Yue, *Adv. Mater.* **2023**, *35*, 2300067.
[233] a) W. He, X. Zhang, C. Jin, Y. Wang, S. Mossin, Y. Yue, *J. Power Sources* **2017**, *342*, 717; b) X. Li, P. Li, X. Liu, S. Luo, Y. Li, X. Su, Y. Zhang, Y. Yue, *J. Non-Cryst. Solids* **2023**, *605*, 122157.
[234] a) Z. Jiang, T. Zhao, J. Ren, Y. Zhang, Y. Yue, *Nano Energy* **2021**, *80*, 105589; b) S. Vaishnav, A. C. Hannon, E. R. Barney, P. A. Bingham, *J. Phys. Chem. C* **2020**, *124*, 5409.

Junwei Ding is a MSCA Postdoctoral Fellow at Aalborg University, Denmark. He received his Ph.D. degree from Beihang University, China in 2020. His research is focused on developing advanced functional materials for zinc, sodium, and lithium batteries.

© 2023 The Authors. Small published by Wiley-VCH GmbH

16136829, 0, Downloaded from https://onlinelibrary.wiley.com/doi/10.1002/smll.202304270 by Aalborg University Library, Wiley Online Library on [06/12/2023]. See the Terms and Conditions (https://onlinelibrary.wiley.com/terms-and-conditions) on Wiley Online Library for rules of use; OA articles are governed by the applicable Creative Commons License

Dongfang Ji is a laboratory technician at Zhengzhou University of Light Industry, China. She obtained her master's degree from Beijing University of Technology, China. Her research is focused on biobased functional materials and their applications.

Yuanzheng Yue is Professor and the leader of the Amorphous Functional Materials Group at Aalborg University, Denmark. His research focuses on glass and amorphous materials. He is Fellow of the European Academy of Sciences, the Royal Society of Chemistry, the Society of the European Ceramics Society, the Society of Glass Technology (UK), and member of the Danish Academy of Natural Science. He is a council member of International Commission on Glass (ICG), the chair of ICG Technical Committee for Glass Fibers. He is an editor of European Journal of Glass Science and Technology and board member of five other journals.

Morten M. Smedskjaer is the group leader and Professor in the Department of Chemistry and Bioscience at Aalborg University, Denmark. He received his Ph.D. degree in materials chemistry from the same university in 2011 and worked as a research scientist at Corning Inc. from 2011 to 2012. His current research focuses on the structure and mechanical properties of oxide and metal–organic framework glasses. He is an editor of Journal of Non-Crystalline Solids. He received an ERC Consolidator Grant in 2022 and is a fellow of the Danish Academy of Technical Sciences and Danish Academy of Natural Sciences.

© 2023 The Authors. Small published by Wiley-VCH GmbH

16136829, 0, Downloaded from https://onlinelibrary.wiley.com/doi/10.1002/smll.202304270 by Aalborg University Library, Wiley Online Library on [06/12/2023]. See the Terms and Conditions (https://onlinelibrary.wiley.com/terms-and-conditions) on Wiley Online Library for rules of use; OA articles are governed by the applicable Creative Commons License